The Canadian Mineralogist
Vol. 39, pp. 1547-1569 (2001)

METAMORPHIC EVOLUTION OF SPESSARTINE QUARTZITES (COTICULES) IN THE HIGH-PRESSURE, LOW-TEMPERATURE COMPLEX AT BAHIA MANSA, COASTAL CORDILLERA OF SOUTH-CENTRAL CHILE

ARNE P. WILLNER[§]

Institut für Geologie, Mineralogie und Geophysik, Ruhr-Universität, D-44780 Bochum, Germany

SABINE PAWLIG[¶]

Institut für Geowissenschaften, Universität Mainz, D-55099 Mainz, Germany

HANS-JOACHIM MASSONNE

Institut für Mineralogie und Kristallchemie, Universität Stuttgart, Azenbergstr. 18, D-70174 Stuttgart, Germany

FRANCISCO HERVÉ

Departamento de Geología, Universidad de Chile, Casilla 13518, Correo 21, Santiago de Chile, Chile

Abstract

Lenses of spessartine quartzites (coticules) are associated with greenschist intercalations in coastal exposures at Bahia Mansa within the mainly metapsammopelitic Western Series, which forms most of the basement in the Coastal Cordillera of central to southern Chile. The chemical compositions of the coticules can be explained by protoliths formed from ferriferous and manganiferous hydrothermal precipitates mixed with aluminous alteration-derived material on top of oceanic crust. The peak conditions of metamorphism were calculated with multivariant reactions: 270–370°C, 6–8 kbar. A retrograde P–T evolution was marked by decompression to 2 kbar during cooling below 300°C, influx of an external fluid, and strain-free crystallization of retrograde phases. The appearance of "ferriwinchite", "ferribarroisite" and phengite in coticules and surrounding metabasic rocks marks the transition from greenschist to epidote blueschist facies. Oscillatory zoning in garnet within the coticules as well as in epidote and tourmaline in the metabasic rocks seems to be governed by the local chemical environment during prograde growth of minerals. Although the garnet in the coticules formed by a continuous prograde dehydration–decarbonation reaction, the primary fluid inclusions are predominantly hydrous owing to massive influx of fluid during the early stage of decompression. The late stage of decompression is bracketed by isochores of primary fluid inclusions that are clearly below peak conditions of metamorphism. This is attributed to a volume increase of the fluid inclusions and stretching of the host minerals during decompression. Higher densities of fluid inclusions in garnet compared to those in quartz are due to differences in yield strength between the two minerals. The transient metamorphic gradient of approximately 12°C/km revealed by the coticules and adjacent metabasic rocks of oceanic origin suggest slow subduction. Penetrative ductile deformation is mainly restricted to the late prograde and early retrograde P–T path within an accretionary prism.

Keywords: coticule, high-pressure, low-temperature rocks, P–T path, Na–Ca amphibole, phengite, oscillatory zoning, fluid inclusions, Coastal Cordillera, Chile.

Sommaire

Des lentilles de quartzite à spessartine (coticules) sont associées à des intercalations de schistes verts dans des affleurements côtiers à Bahia Mansa de la séquence à dominance métapsammopélitique (série de l'Ouest) qui constitue la plupart du socle de la Cordillère Côtière des parties centrale et australe du Chili. La composition chimique des coticules peut s'expliquer à partir de contributions de protolithes formés de précipités hydrothermaux ferrifères et manganifères, mélangés à des matériaux alumineux dus à l'altération de la partie supérieure de la croûte océanique. Les conditions maximales de métamorphisme ont été calculées au moyen de réactions multivariantes: 270–370°C, 6–8 kbar. Une évolution P–T rétrograde a été marquée par une décompression jusqu'à 2 kbar et d'un refroidissement à moins de 300°C, la venue d'une phase aqueuse d'une source externe, et d'une

§ *E-mail address*: arne.willner@ruhr-uni-bochum.de
¶ née Lange

cristallisation des phases rétrogrades sans déformation. L'apparition de la "ferriwinchite", la "ferribarroisite" et la phengite dans les coticules et les roches métabasiques encaissantes signale une transition à partir du faciès schistes verts au faciès schistes bleus à épidote. Une zonation oscillatoire dans le grenat des coticules, de même que dans l'épidote et la tourmaline des roches métabasiques, semble résulter du milieu chimique local au cours de la croissance prograde des minéraux. Quoique le grenat des coticules s'est formé par une réaction prograde continue impliquant déshydratation et décarbonation, les inclusions fluides primaires sont en majorité aqueuses à cause d'une infiltration massive de fluide au cours du stade précoce de la décompression. La stade tardif de la décompression est délimité par les isochores définis par les inclusions fluides primaires, qui sont nettement inférieures aux conditions maximales atteintes au cours du métamorphisme. Ces conditions seraient dues à l'augmentation du volume des inclusions fluides et un étirement des minéraux hôtes pendant la décompression. Les densités supérieures des inclusions piégées dans le grenat, par rapport à celles des inclusions piégées par le quartz, seraient dues aux différences dans le seuil de déformation entre ces deux minéraux. Un gradient métamorphique transitoire d'environ 12°C/km, révélé par les assemblages des coticules et des roches métabasiques adjacentes d'origine océanique, font penser à un milieu de subduction lente. Une déformation ductile pénétrante est surtout limitée au stade tardif de la recristallisation prograde et au stade précoce de la recristallisation rétrograde au cours de l'évolution P–T dans un prisme d'accrétion.

(Traduit par la Rédaction)

Mots-clés: coticule, roches de haute pression et de faible température, évolution P–T, amphiboles Na–Ca, phengite, zonation oscillatoire, inclusions fluides, Cordillères Côtières, Chili.

Introduction

Rocks consisting mainly of quartz and spessartine-rich garnet, *i.e.*, spessartine quartzites, are generally known under the loosely defined term "coticules" (Renard 1878; French for "whetstone", referring to its original industrial use; see also Spry 1990). They are mostly hosted in metapelites and commonly occur in close association with stratiform massive sulfide deposits and rocks of hydrothermal origin (exhalites) such as tourmalinite, iron formations, and Zn- or Ba-rich rock types (Spry 1990, Krosse & Schreyer 1993, Spry *et al.* 2000). They are typically exposed as thin layers or lenses in metamorphic complexes of very low to high grades and variable ages. Owing to their conspicuous pale color and sharp contacts with their host rocks, they are easily detectable in the field. Because primary sedimentary structures are mostly absent, the origin of coticules has been a matter of debate in the past. They are generally taken as an indicator for the proximity of metamorphosed base-metal, scheelite and gold deposits (Spry *et al.* 2000).

In this paper, we describe such rocks from a belt of low-grade metamorphic rocks exposed within the Coastal Cordillera in Chile, south of latitude 32ºS, that has been interpreted as a system of accretionary complexes (Hervé 1988, Massonne *et al.* 1996). In this belt, a rather unique opportunity exists to study processes related to pre-Andean subduction and high-pressure metamorphic rocks at the South American convergent margin. In detail, our aims are to: (1) determine the genesis of coticules in a geodynamic environment characterized by a high-pressure – low-temperature metamorphic imprint, in a setting where they were not described previously, (2) derive a P–T path in relation to fluid evolution, reaction and deformation history of the host rocks, and (3) compare metamorphic evolution with that of the surrounding rock-types, which are characterized by mineral assemblages transitional between greenschist and blueschist facies.

Geological Setting

Two major series of metamorphic rocks are distinguished within the basement of the Coastal Cordillera in Chile (Aguirre *et al.* 1972, Hervé 1988; Fig. 1). The Western Series consists of transposed, low-grade phyllites and metagreywackes with intercalated lenses of greenschists and, locally, blueschists. The Eastern Series consists of less penetratively deformed, very-low-grade metagreywackes and metapelites, with preserved sedimentary structures and stratigraphic continuity in outcrop scale, and lacking any intercalation of metabasic rocks. This association is generally interpreted as a transition from deformed forearc-basin sediments exposed in the east of the Coastal Cordillera to an accretionary complex in the west (Kato 1985, Hervé 1988, Martin *et al.* 1999, Willner *et al.* 2000). In central and south-central Chile, rocks of the Eastern Series were incorporated into an Upper Paleozoic magmatic arc with local superimposition of low-pressure and medium- to high-temperature metamorphism. The Western and Eastern series in this part of Chile were interpreted as a paired metamorphic belt by Aguirre *et al.* (1972). Boundaries between the series are dextral strike-slip faults separating different lithological associations, metamorphic grades and structural trends (*e.g.*, Martin *et al.* 1999).

In south-central Chile, *i.e.*, in the broad surroundings of our study area, rocks of the Western Series predominate, because those of the Eastern Series are covered mostly by Mesozoic sediments (Fig. 1). There, the Western Series consists of two sequences of different origin: (1) mostly polycyclic metagreywackes of average shield composition, which can be considered to be typical of continental rocks (Schira *et al.* 1990), and (2) slices of a "dismembered ophiolite sequence" (Hervé

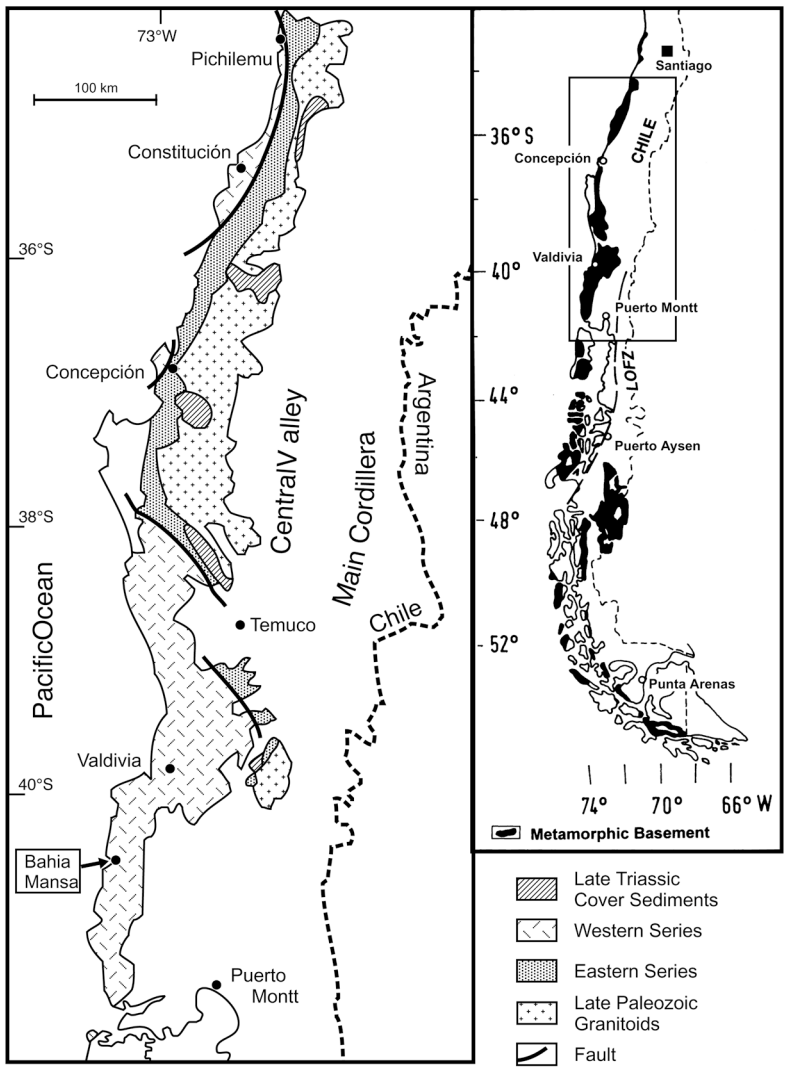

FIG. 1. Geological map of the basement of the Chilean Coastal Cordillera between 34° and 42°S (after Martin *et al.* 1999).

1988, Schira *et al.* 1990, Collao *et al.* 1990). The "ophiolite sequence" is mainly composed of m- to km-scale lenticular bodies of greenschists derived from oceanic tholeiites with N–MORB or E–MORB character, but partly also with calc-alkaline and alkali basalt affinities (Schira *et al.* 1990, Kato & Godoy 1995) and a few bodies of serpentinized peridotite. Small lenticular orebodies are intercalated on a meter-scale with the greenschists. The orebodies are massive Fe–Cu–Pb–Zn sulfides and banded iron-formations. The latter contain variable proportions of magnetite, stilpnomelane, blue-green amphibole, quartz, and garnet. Rare cm-thick bands of tourmalinite associated with the metabasites are believed to have originated from exhalative processes (Schira *et al.* 1990, Collao *et al.* 1990).

In the Western Series, between latitudes 38º and 42ºS, the regional structural trend is consistently NW–SE, thus oblique to the NNE–SSW-trending morphology of the Andes (Kato 1985, Schira *et al.* 1990, Martin *et al.* 1999). The predominant S_2 foliation, containing relict S_1 and rootless isoclinal F_1 fold hinges, transposed all earlier structures and is parallel to the axial plane of recumbent cm- to m-scale F_2 folds. Fold axes and stretching lineations are parallel to the general NW–SE trend. S_2 is refolded by large-scale open F_3 folds.

Abundant indicators of high-pressure metamorphism in the Western Series have been observed, such as glaucophane (Kato 1985, Kato & Godoy 1995), zussmanite (Massonne *et al.* 1998), cymrite (Muñoz & Hervé 2000), and widespread phengite with a Si-rich core (Massonne *et al.* 1996). Applying the sphalerite geobarometer, Collao *et al.* (1986) estimated pressures of 4.4–9.0 kbar in massive sulfides at Pirén Alto. Nevertheless, most of the rocks are believed to be entirely overprinted by a late lower-greenschist facies event (*e.g.*, Kato 1985, Martin *et al.* 1999). This latter view is contradicted in this paper.

The age of deposition for the metapsammopelites in the Western Series of south-central Chile may be partly as young as Permian, according to the youngest concordant U/Pb age of detrital zircon at 275 Ma (Duhart *et al.* 1997). This finding agrees with widespread K/Ar ages between 220 and 250 Ma based on white mica and amphibole, which likely date the onset of exhumation (Duhart *et al.* 1997). Ages for phengite in glaucophane-bearing assemblages (304 Ma, K/Ar by Kato & Godoy 1995; 324 Ma, Ar/Ar by Kato *et al.* 1997) are considerably older. Granites intruding the Eastern Series at the same latitudes yielded U/Pb ages of 282–306 Ma (Martin *et al.* 1999). These authors suggested a two-stage geodynamic evolution, involving construction of a late Paleozoic paired metamorphic belt with a coeval magmatic arc and a Late Permian to Late Triassic exhumation and emplacement of the Western Series within a dextral transpressional setting. The oldest sediments, which unconformably overly the basement rocks, are marine to terrestrial siliciclastic rocks of Late Triassic age (Martin *et al.* 1999).

Field Occurrence and Petrography

In this study, we concentrate on coticule intercalations within a major occurrence of greenschists, several hundred m thick at Playa Tril–Tril, 4 km south of Bahia Mansa (WGS84: 40°36.77'S, 73°45.20'W). The coticules form conspicuous, pale lenses or layers 5 to 10 cm thick that are laterally continuous at outcrop scale. They alternate with greenschists and, more rarely, dark pelitic schists over several tens of meters in coastal outcrops. No primary sedimentary structures were detected, but the contacts with the surrounding rocks are sharp. Occasionally, mm- to dm-thick layers or lenses of magnetite are also intercalated with the greenschists. Similar intercalations of strings of pyrite (cm to dm scale) are observed in the dark pelitic intercalations. Lithological layering is subparallel to the predominant foliation that produces a penetrative banding in all rock types and represents the penetrative S_2 transposition foliation, as described by Kato (1985) and Schira *et al.* (1990). Some layers of greenschists (cm to m thick) have a spotted appearance owing to abundant mm-size albite porphyroblasts.

Coticules

The predominant assemblage of the coticules (samples 96CH–193, –197, –199, –201, –207, –209, –213) is quartz – garnet – stilpnomelane – chlorite – carbonate – white mica ± amphibole ± titanite ± pyrite (Fig. 2A). Albite, apatite and epidote are occasional accessory phases. Most typical is a sharp thin metamorphic banding with alternating quartz-rich bands and bands 0.05–1 mm thick enriched in tiny idioblastic crystals of garnet (diameter <80 μm; Figs. 2B, C). The garnet crystals form a typical polygonal fabric and can be intergrown with oriented grains of stilpnomelane and rare white mica, chlorite, titanite, or blue-green amphibole. Some garnet bands show rootless isoclinal fold closures with enrichment of garnet in the hinge zone, where layer silicates recrystallized mimetically. Amphiboles generally show a blue-green core and green rim oriented parallel to the predominant foliation. Quartz layers are characterized by a polygonal recrystallization fabric with heterogeneous distribution of grain size (100–800 μm) and include some carbonate, scattered idioblastic pyrite, apatite or garnet grains, as well as unoriented stilpnomelane. Garnet grains occur in mutual contact with carbonate (Fig. 2C).

Greenschists

The predominant assemblage in the metabasites (samples 96CH191, –194, –196, –214, –215, –217, –219) is albite – amphibole – chlorite – epidote – white mica – titanite ± quartz ± calcite ± magnetite ± tourmaline ± apatite. The degree of orientation of amphibole, chlorite, epidote, and white mica grains varies strongly. Where microfold hinges are preserved, recrystallization is evident. Abundant xenoblastic albite porphyroblasts, up to 1 mm in size, overgrew these F_2 fold hinges as the latest phase. These porphyroblasts enclose mainly epidote and titanite and minor amphibole. Blue-green amphibole exhibits irregular color zoning, with a bright bluish color mostly in the core to darker bluish and finally green at the rim.

Layers of pure epidosite of mm to dm thickness or epidote–chlorite rocks are common. Epidote generally shows optical zoning. Also, strings or veinlets of magnetite, calcite, unoriented white mica, chlorite or quartz up to 0.8 mm across are abundant.

Greenschist sample 96CH–214 contains a rare mm thick, discontinuous layer of tourmalinite with a polygonal fabric of small green tourmaline crystals (<40 μm grain size; Fig. 2D).

Quartz phyllite

This dark metapsammopelitic rock (sample 96CH–192) is characterized by a pronounced alternation of mm-size quartz-rich bands and dark bands enriched in

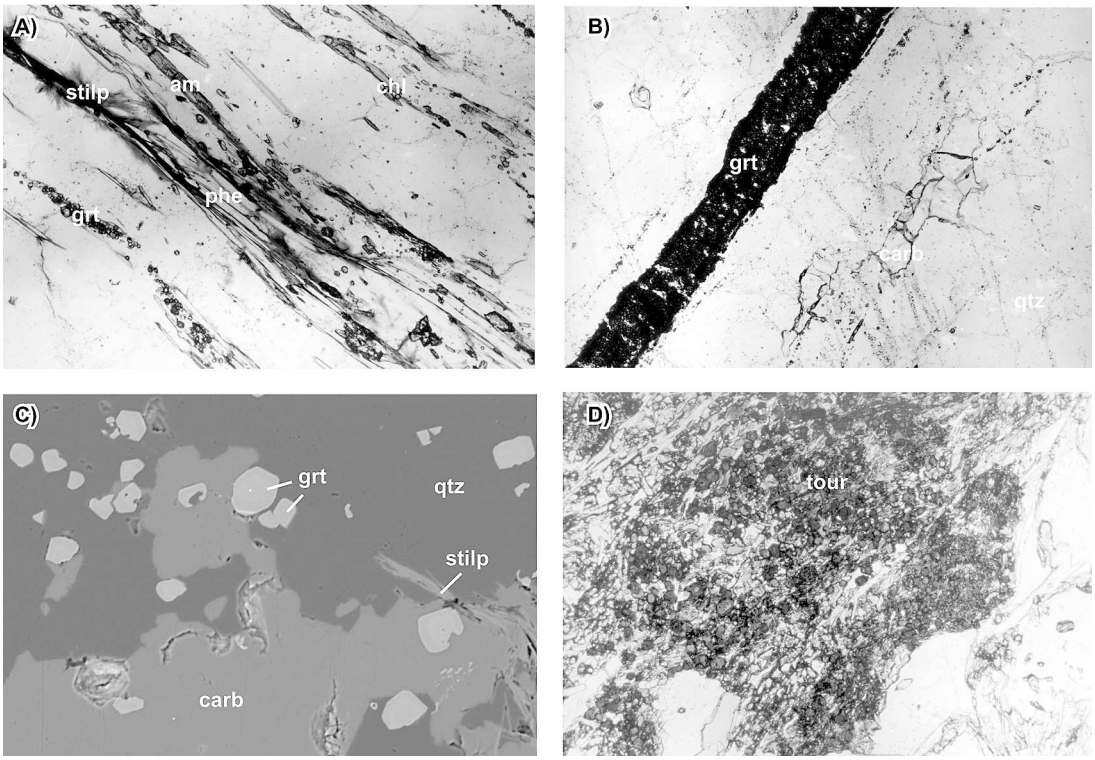

FIG. 2. A. Typical coticule assemblage quartz – garnet – amphibole – phengite – stilpnomelane – chlorite – pyrite. Sample 96CH–197. Plane-polarized light. Width of the photo is 4 mm. B. Band of polygonal garnet aggregates alternating with quartz–carbonate bands containing minor garnet in coticule sample 97. Plane-polarized light. Width of the photo is 3 mm. C. Detail BSE image from Fig. 2B with the stable assemblage quartz – carbonate – garnet. Note zoning in garnet. Width of image is 0.5 mm. D. Tourmalinite layer in greenschist sample 96CH–214 showing oriented Ca–Na–amphibole, epidote, chlorite and phengite. Width of the photo is 4 mm.

strongly oriented white mica, chlorite, and graphite. Biotite is absent. A pyrite-rich lens is oriented parallel to the banding. S_2-crenulation hinges contain mimetic recrystallization of the phyllosilicates. Quartz grains or aggregates are strongly elongate with curved grain-boundaries in the phyllosilicate bands, suggesting pronounced pressure-solution. Quartz and rare albite show a polygonal fabric, with up to 800 μm grain size in the quartz-rich bands.

Chlorite–amphibole mica schist

This rock type (sample 96CH–205) transitional between metapsammitic and metabasic rocks is also strongly banded, with oriented blue-green amphibole, epidote, titanite, white mica and chlorite enriched in the dark bands alternating with quartz–albite-rich bands with a polygonal fabric. Albite porphyroblasts overgrew the dark bands enclosing white mica and epidote.

ANALYTICAL METHODS

Whole-rock chemical analyses were made with a Philips PW 1404 X-ray fluorescence spectrometer using Rh radiation and operated at 85 kV, 35 mA for the trace elements and Fe, and 40 kV, 75 mA for major elements. Results are listed in Table 1.

Minerals were quantitatively analyzed in wavelength-dispersion mode with a JEOL JXA 8900 RL electron microprobe operating with an acceleration voltage of 15 kV and a beam current of 12 nA. The raw data were corrected with an Oxide–PRZ procedure. Wollastonite (Si, Ca), orthoclase (K), albite (Na), periclase (Mg), hematite (Fe), corundum (Al), synthetic Cr_2O_3 (Cr), pyrophanite (Mn, Ti), barite (Ba), tugtupite (Cl) and F-substituted phlogopite (F) served as standards. Representative results are listed in the appendix, which also contains the mode of calculation of structural formulae. Further compositions will be provided by the

TABLE 1. BULK-ROCK COMPOSITIONS OF COTICULES FROM BAHIA MANSA, CHILE, AND FROM THE ARDENNES, WESTERN GEORGIA, TRONDHEIM AND BROKEN HILL

Sample	96CH -193	96CH -197	96CH -199	96CH -201	96CH -207	96CH -209	96CH -213	Mean	Ardennes Belgium	W. Ga	Trond-heim	Broken Hill
SiO_2 wt.%	89.12	89.62	83.13	91.84	89.26	89.62	91.30	89.13	58.90	49.20	55.90	63.95
TiO_2	0.08	0.16	0.28	0.13	0.14	0.12	0.07	0.14	1.05	0.23	0.47	0.52
Al_2O_3	2.73	3.09	5.09	2.37	2.98	2.94	2.63	3.12	20.28	8.13	10.8	11.45
FeO_{total}	2.48	2.60	3.50	2.44	2.97	2.73	2.30	2.79	1.71	24.99	13.70	7.31
MnO	3.12	1.25	5.34	0.76	2.26	2.35	2.35	2.49	9.83	11.5	6.02	3.69
MgO	0.51	0.71	0.80	0.71	0.86	0.76	0.52	0.70	1.40	0.31	1.70	0.19
CaO	0.68	0.72	1.14	0.50	0.70	0.74	0.66	0.73	0.24	1.68	5.30	10.77
Na_2O	0.13	0.28	0.07	0.35	0.17	0.02	0.06	0.15	0.71	0.01	0.30	0.06
K_2O	0.13	0.57	0.05	0.41	0.06	0.04	0.05	0.19	2.60	0.11	0.10	0.77
P_2O_5	0.17	0.02	0.07	0.02	0.15	0.18	0.09	0.10	0.07	0.09	0.29	0.05
LOI	0.42	0.74	0.41	0.64	0.58	0.48	0.29	0.51	2.57	1.39	n.d.	0.16
Total	99.57	99.76	99.88	100.18	100.14	99.99	100.30	100.05	99.36	97.64	94.58	98.92
Sc ppm	3	4	6	3	4	5	3	4	nd	nd	nd	nd
V	81	45	51	7	74	61	61	59	91	12	49	nd
Cr	35	21	22	20	27	27	29	26	113	32	293	nd
Ni	98	8	140	32	73	57	66	68	68	17	43	nd
Cu	112	135	194	73	127	32	57	104	15	1	140	0
Zn	50	43	47	46	69	54	38	55	97	39	53	100
Ga	4.9	5.9	6.0	5.3	4.7	4.4	4.5	5	28	nd	nd	nd
Rb	7	21	3	15	4	2	3	9	122	10	12	nd
Sr	15	37	12	30	12	12	8	18	149	8	57	nd
Y	25	12	21	10	21	23	17	18	39	18	28	nd
Zr	25	40	42	36	39	40	26	39	157	24	86	nd
Nb	3	5	7	4	5	5	3	5	18	20	15	nd
Ba	61	1403	25	1058	41	18	27	376	691	140	nd	nd

Ardennes, Belgium (Krosse & Schreyer 1993), n = 23; W. Ga: western Georgia, U.S.A. (Wonder *et al.* 1988); Trondheim: Trondheim area, Norway (Bjerkgard & Bjorlykke 1996); Broken Hill: Broken Hill, Australia (Spry & Wonder 1989).

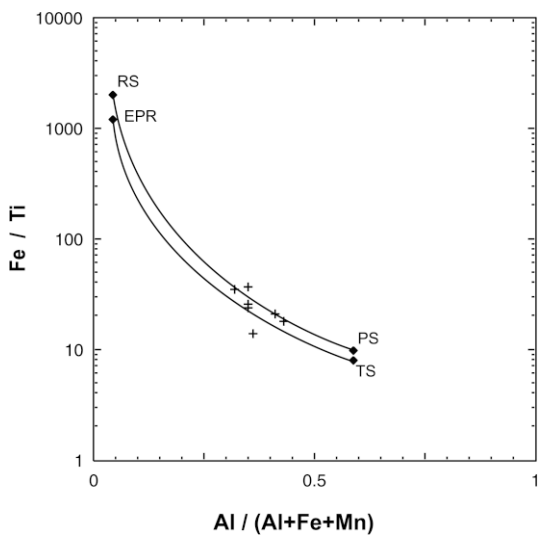

FIG. 3. Composition of coticules (crosses) in terms of Fe/Ti *versus* Al/(Al + Fe + Mn) (after Spry 1990). Curves represent mixtures of sediments from the East Pacific Rise (EPR), the Red Sea (RS), with terrigenous (TS) and pelagic (PS) sediments.

first author upon request or can be taken from Lange (1997).

To reveal compositional inhomogeneities involving the major elements (Fe, Mg, Ca, Mn) in optically uniform grains of garnet, element-distribution maps were produced. Step lengths of the scans were set at 0.1–1 μm, depending on the desired spatial resolution, size of the individual grains and the available time for measurement. Scans over areas of 0.5 mm^2 thus typically contain 250000 pixels. Counting times of 0.1–0.5 seconds per step at 15 kV acceleration voltage and 12 nA beam current resolve even minor concentration-gradients in the garnet.

Microthermometric analyses of fluid inclusions in garnet and quartz of the coticules were obtained with a Linkam TH600 heating–freezing stage. Heating rates used to determine the homogenization temperatures were 10°C/min and 0.1°C/min to determine the freezing temperatures. Reproducibility was ±0.3°C for freezing temperatures and ±0.5°C for homogenization temperatures. To identify small amounts of CO_2 in the H_2O-rich inclusions in quartz, infrared spectra were recorded using a Perkin Elmer 1760 FT–IR spectrometer.

Whole-Rock Geochemistry of the Coticules

The chemical composition of seven spessartine quartzites from Bahia Mansa are shown in Table 1. As in other occurrences of coticules world-wide, there is a strong deficiency in alkalis compared to pelitic or basic rocks; Si, Al, Fe, Mn and Ca are the most abundant elements. SiO_2 contents of the Bahia Mansa samples are around 83–91 wt%, among the highest known for coticules according to Spry *et al.* (2000). A positive correlation of TiO_2 *versus* Al_2O_3 can be observed, as is typical in most coticules and attributed to a detrital contribution (Slack *et al.* 2000). In a plot of Fe/Ti *versus* Al/(Al + Fe + Mn) (Fig. 3), all coticules including our Bahia Mansa samples fall onto the mixing line between pelagic clays and hydrothermal metalliferous precipitates, as established by Bonatti (1975; see also Spry 1990, Spry *et al.* 2000). However, the contribution of the hydrothermal component seems to be relatively minor. As in most coticules, (Co + Cu + Ni) × 10 is low relative to Fe and Mn (Fig. 4); the rocks thus resemble hydrothermal precipitates rather than hydrogenous sediments, which form by extremely slow precipitation from seawater (Bonatti 1975, Spry 1990). This is in line with increased Ba concentrations in some Bahia Mansa coticules. Compared to other coticules (Table 1), the Bahia Mansa samples show a slight deficiency with respect to Ti, Zr, Cr, Y and Nb, presumably because of a low proportion of a terrigenous detrital component. Similarities in mineral assemblages and spatial association with surrounding greenschists could also indicate hydrothermal alteration and associated concomitant precipitation within a tuffaceous protolith, as proposed by Kramm (1976) for coticules in Belgium. It must be noted that any hydrothermal precipitation is related to concomitant alteration generating Al-enriched material from precursor pelites or tuffs (Brimhall & Crerar 1987). Coticules hence are a mixture of products of both processes, as presumably are most of the associated metaexhalites.

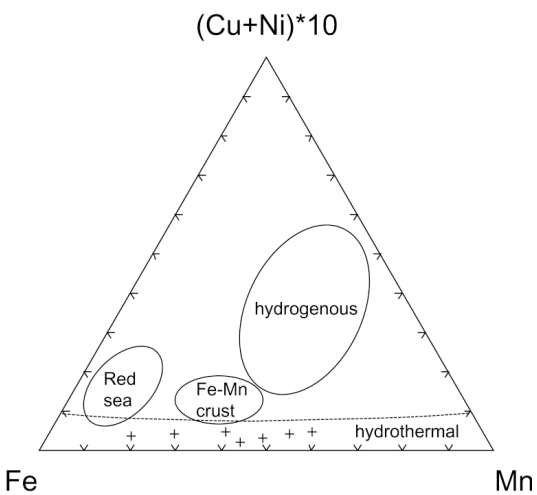

FIG. 4. Composition of coticules (crosses) in terms of (Cu + Ni) × 10 – Fe – Mn after Bonatti (1975), with fields for sediments from the Red Sea, hydrogenous (seawater precipitates), hydrothermal material and Mn-rich crust.

Pyrite is the only nonsilicate in the coticules, whereas magnetite is present in the surrounding metabasic rocks; the presence of pyrite could point to lower fugacity of oxygen within the original environment of formation, as also observed for example by Kramm (1976) in the Ardennes, where surrounding very-low-grade rocks still contain abundant hematite. More reducing fluids present during precipitation of the coticule protoliths thus would have been responsible for the concentration of Mn relative to Fe, as proposed by Bonatti (1975). Bonatti assumed that hydrothermal (Fe,Mn)-rich solutions became oxidized by seawater. Proximal precipitates would be Fe^{3+}-rich (possible protoliths of stilpnomelane-bearing quartzites and stilpnomelane enrichments in the greenschists), whereas Mn was transported to more distal, reducing areas, being precipitated during formation of the protoliths of the coticules.

Mineral Chemistry

White mica

All analyzed samples of white mica consist of phengite (see Appendix) showing a variation from 3.18 to 3.5 Si per formula unit without difference among the rock types studied (Fig. 5). Most compositions plot below the ideal Tschermak-substitution line in Figure 5 owing to partial substitution of Al by Fe^{3+} (0–0.37 atoms per formula unit, *apfu*) or of 2 Al by R^{2+} + Ti (Ti between 0.006 and 0.046 *apfu*). Values of X_{Mg} [= Mg/(Fe^{2+}+ Mg)] range between 0.5 and 0.7 regardless of rock type. Furthermore, no clear pattern of chemical zonation was observed in individual grains, but low values of Si are generally measured near the rim. Although the paragonite component is generally low (5–17 mole %), there is a remarkable content of Ba in all samples (0.2–4.3 wt% BaO; 0.03–0.24 Ba *apfu*). These unusually high Ba-contents indicate a premetamorphic similarity among the rock types studied. A Ba-bearing hydrothermal fluid presumably affected the protoliths of all rock types.

Garnet

Garnet occurs in the coticules only (see Appendix). It is rich in spessartine (45–80 mole %), with variable amounts of grossular (9–20 mole %) and almandine (2–30 mole %). Proportions of andradite (2–15 mole %) and pyrope (≤ 2 mole %) components are low. The clear

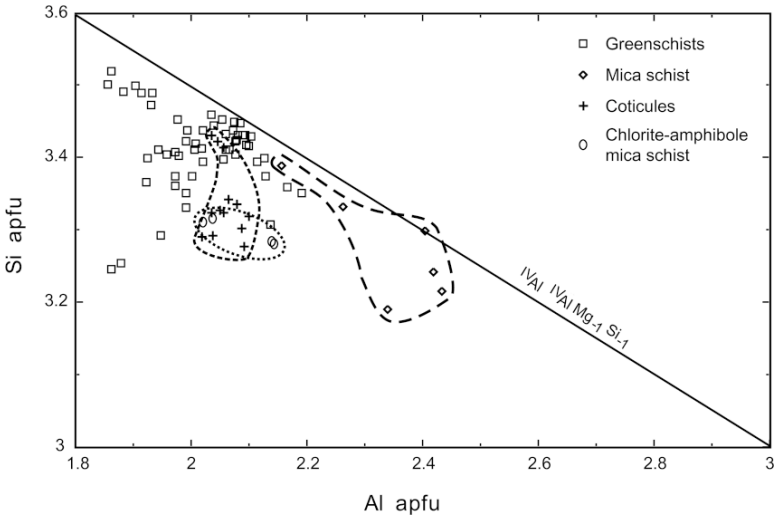

FIG. 5. Plot showing Si *versus* Al for phengite compositions. The line of ideal Tschermak substitution is indicated.

pattern of zonation indicates prograde growth. The proportions of spessartine and andradite components decrease from the core to the rim (Figs. 6, 7, 8), whereas contents of almandine, pyrope, grossular and X_{Mg} increase in the same direction. Back-scattered electron (BSE) images, element-distribution maps and scans through single crystals reveal growth zonation, with euhedral zones around a small anhedral core (Figs. 6, 7). Chemical zoning is oscillatory, as shown in BSE images; zoning is only reflected in the distribution map for Ca, however. Two oscillatory zones are generally observed, but the zones of relative Ca-enrichment do not correlate with any distinct changes in proportion of Mg, Fe or Mn components. The local increase in Ca thus is simultaneously compensated by all other elements. Furthermore, the Ca oscillatory pattern is not symmetrical on either side of the core.

Carbonate

Although calcite is the only carbonate in metabasic rocks (see Appendix), up to three carbonates coexist with spessartine in the coticules: siderite ($cal_{0.08–0.14}sd_{0.59–0.76}mgs_{0.00–0.02}rds_{0.15–0.29}$), calcite ($cal_{0.87–0.95}sd_{0.01–0.06}mgs_{0.00–0.03}rds_{0.02–0.08}$) and dolomite ($cal_{0.53}sd_{0.06}mgs_{0.41}$). Siderite is by far the most abundant, and dolomite, the least abundant carbonate. The wide solid-solution gap among the carbonates (Fig. 6) is consistent with the experimental studies of the system $CaCO_3$–$FeCO_3$ at low temperatures by Rosenberg (1963). Element distribution within carbonate grains does not show any systematic zonation.

Amphibole

Amphiboles (see Appendix) occur in all rock types: blue-green Na-rich amphibole compositions occur in the amphibole cores, whereas actinolite is present in the rim and as small discrete crystals. There is a continuous transition between the two amphiboles: ^{B}Na (= ^{M4}Na) varies from 0.64 to 1.20 *apfu* in the Na-rich amphibole portion [(ferri)-winchite with Si 7.50 – 7.93 *apfu* and (ferri)-barroisite with Si 7.24–7.50 *apfu*; amphibole terminology according to Leake *et al.* 1997] and 0.10 to 0.64 *apfu* in the actinolite (Si 7.50–7.99 *apfu*), whereas X_{Mg} ranges from 0.60 to 0.80 in all amphiboles (Fig. 9A). There is a negative correlation between $^{B}Na/(^{B}Na + Ca)$ and Si (Fig. 9B), which suggests concomitant winchite and Tschermak substitutions, presumably reflecting P and T changes during amphibole growth. Also a single grain of magnesioriebeckite was analyzed in coticule sample 96CH–197. Fe^{3+} contents of 0.70–1.33 *apfu* and X_{Fe3+} [= $Fe^{3+}/(Fe^{3+} + {}^{VI}Al)$] of 0.72–0.92 in "ferriwinchite" and "ferribarroisite" point to an oxidized environment, as does the high-Fe epidote. Fe^{3+} contents are lower in actinolite ($0.1 < Fe^{3+} < 0.8$, $0.30 < X_{Fe3+} < 0.93$). The *A* position is occupied by 0.04–0.33 *apfu* $^{A}Na + K$ in the ferribarroisite. The occupancy is generally lower in ferriwinchite (0.00–0.17 *apfu*) and actinolite (0.00–0.15 *apfu*). Although there is a marked solid-solution gap between actinolite and glaucophane up to temperatures of at least 350°C (Maruyama & Liou 1988), the continuous winchite substitution $Ca + R^{2+} = {}^{B}Na + R^{3+}$ as observed in actinolite, "ferriwinchite" and "ferribarroisite" of our low-grade samples proves the exist-

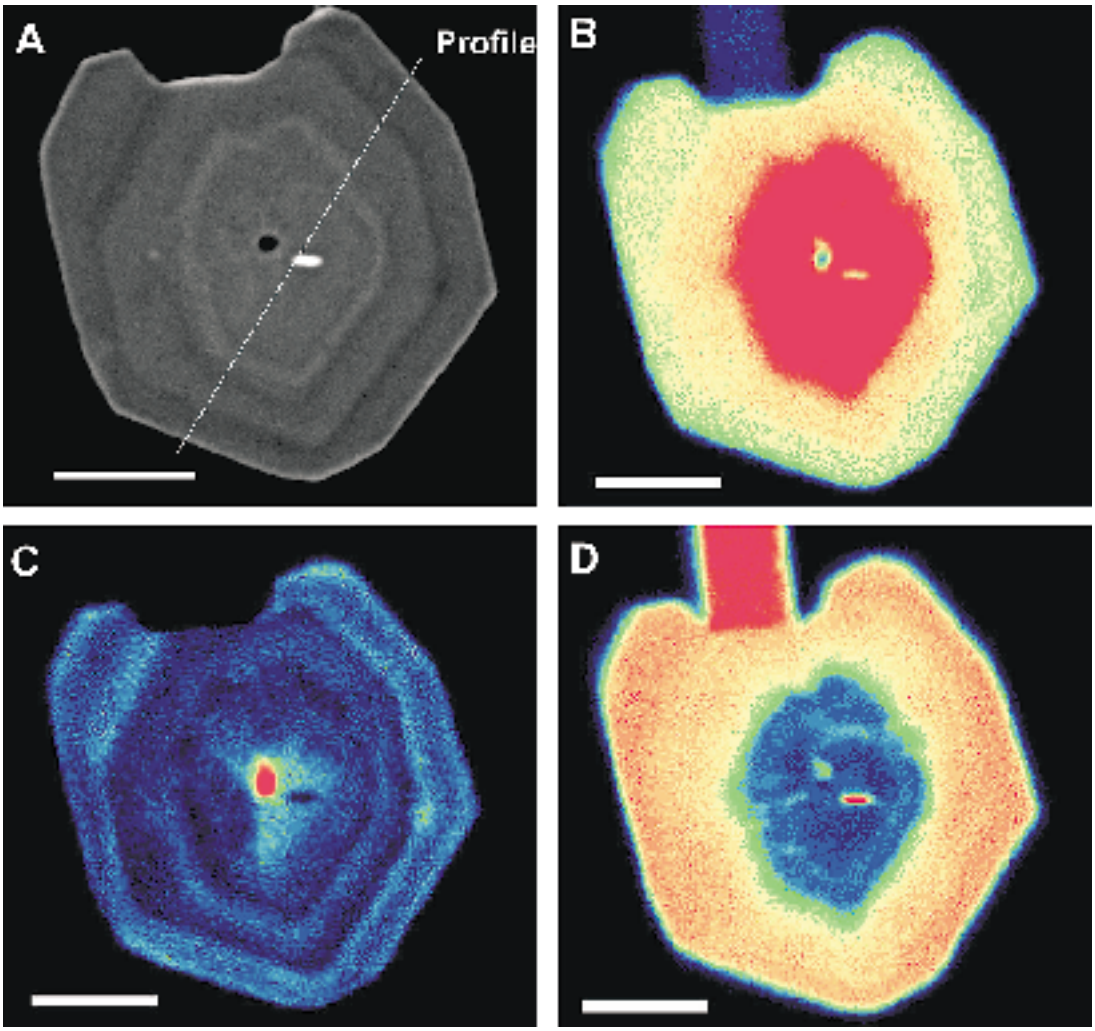

FIG. 6. A. Back-scattered electron image of garnet (coticule sample 96CH–207). B. Map of X-ray intensity distribution for Mn. C. Map of X-ray intensity distribution for Ca. D. Map of X-ray intensity distribution for Fe^{2+}. Scale is 10 μm. Relative intensities increase in the order blue – green – yellow – red.

ence of a complete solid-solution between actinolite and magnesioriebeckite (Fig. 10), as also observed by El Shazly *et al.* (1990) and Massonne (1995a), for example. Mn contents of the "ferriwinchite" and actinolite are higher in the coticules (0.09–0.16 *apfu*) than in the surrounding rock types (0.02–0.09 *apfu*). Within the Na-rich amphibole portions, no clear pattern of zonation could be observed. It must be noted that use of the informal name "ferriwinchite" (thus the quotation marks) is problematic, because it shows an apparent inconsistency with the current amphibole nomenclature (Sokolova *et al*. 2001). "Ferribarroisite" also is not yet an IMA-approved species.

Titanite

Titanite exists as an accessory phase in all samples. It shows a uniform composition (see Appendix) with a $Ca(Al,Fe^{3+})SiO_4(F,OH)$ component between 5.4 and 14.5 mole %. Only the titanite in the coticules contains considerable Mn contents, up to 0.35 wt% MnO, and 0.1–0.7 wt% F is common for titanite of all samples.

Stilpnomelane

Stilpnomelane is omnipresent in the coticules, but was found in only one metapsammopelitic sample.

There is a variation of X_{Fe3+}, here defined as $Fe^{3+}/(Fe^{3+} + Fe^{2+})$, between 0.02 and 0.11, and X_{Mg} between 0.30 and 0.41. Notable are the relatively high contents of Mn (4.0–6.2 wt% MnO) and Ba (0.20–0.96 wt% BaO).

Chlorite

Chlorite (see Appendix) is ubiquitous in all samples without clear internal chemical zonation. Chlorite grains in the coticules show considerably higher Mn contents (0.16–0.55 *apfu*) than those of the surrounding rocks (0.04–0.16 *apfu*). The X_{Mg} value of chlorite in the metabasic rocks (0.44–0.62) is more variable in metapsammopelites (0.42–0.44) and the coticules (0.46–0.54), whereas the Si content of chlorite of all samples studied ranges from 5.46 to 5.93 *apfu*.

Epidote

Epidote (see Appendix) occurs in all samples and contains 50 to 99 mole %, (mostly above 80%) of the "pistacite" component. Distribution of Fe within the grains is rather irregular. However, BSE images of single crystals show a clear pattern of oscillatory growth, mostly in two cycles, with increasing Fe^{3+} (brighter zones in Fig. 11) toward the rim and a narrow discontinuous and anhedral outermost rim with the highest "pistacite" component. Some grains show a small, anhedral core, also with a high "pistacite" content. The distribution pattern of Mn varies widely within rock types and within individual grains (0.07–0.47 wt% Mn_2O_3 in greenschists and 0.88–1.0 wt% Mn_2O_3 in coticules).

Plagioclase

Plagioclase is most common in the metabasic rocks and metapsammopelites, but it also occasionally occurs as an accessory phase in the coticules. It is virtually pure albite with <0.5 mole % of anorthite + orthoclase component; the only significant minor oxide is Fe_2O_3 (<0.3 wt%).

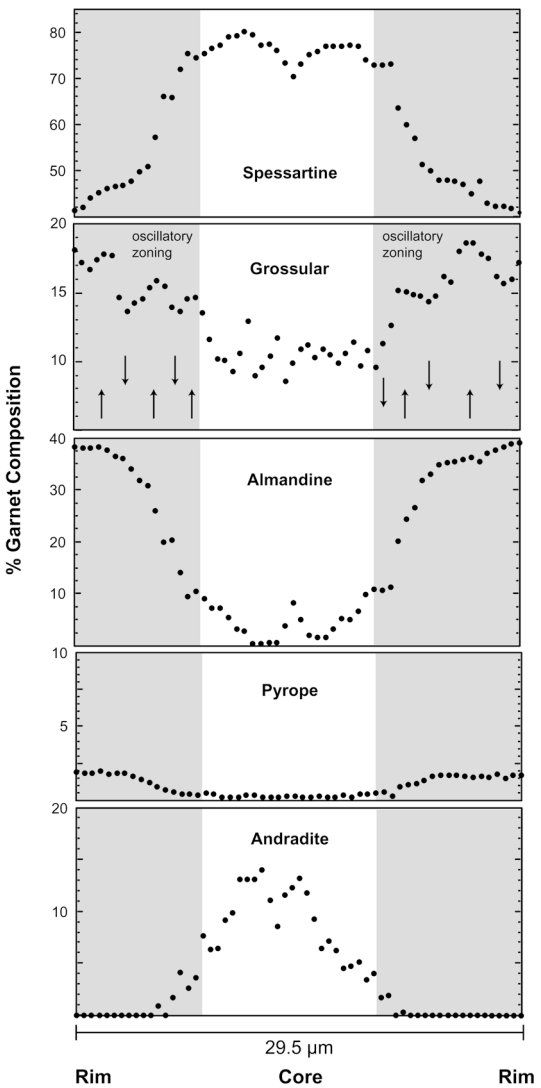

FIG. 7. Quantitative scan through the garnet grain in Figure 6. Arrows indicate direction of small scale change in grossular component. They correspond to features observed in Figure 6.

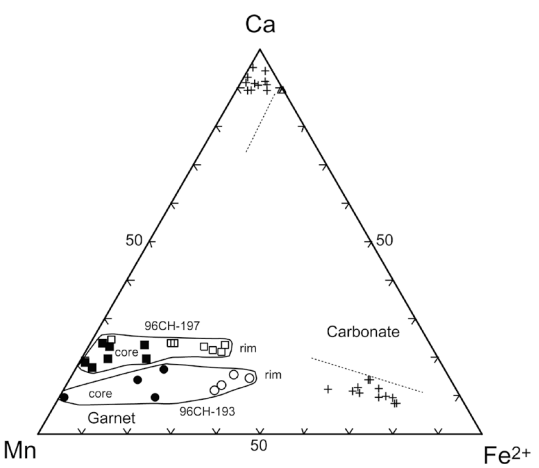

FIG. 8. Ca–Fe–Mn plot of garnet and carbonate compositions. Note the solid-solution gap between calcite and siderite. Symbols: squares and crosses: sample 96CH–197, circles: sample 96CH–193, filled symbols: core compositions; open symbols: rim compositions.

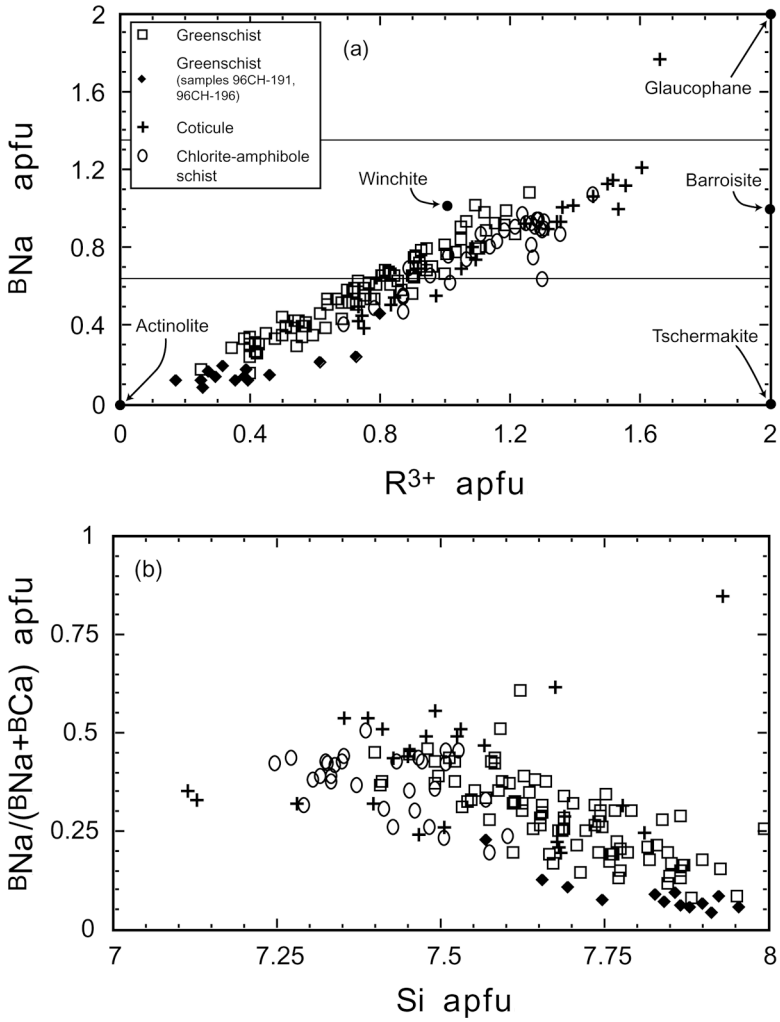

FIG. 9. A. ^{B}Na *versus* R^{3+} variation in amphiboles. B. ^{B}Na/(^{B}Na + Ca) *versus* Si variation.

Tourmaline

Tourmaline is present in narrow mm-thick layers of tourmalinite in one sample of metabasic rocks (96CH–214). It represents a dravite–schorl solid solution with a range of X_{Mg} between 0.48 and 0.62, which is typical of tourmalinites in general (Henry & Dutrow 1996). Tourmaline grains from Bahia Mansa also show a distinct pattern of zonation in BSE images. The pattern is similar to that observed in garnet and epidote (Fig. 11). A small, homogeneous and anhedral nucleus is surrounded by a broad rim with euhedral, asymmetrical and oscillatory growth-zones. Again, two cycles of oscillation can be detected. All core zones have the same chemical composition throughout the sample. A detrital origin of the cores would likely show markedly different compositions to the rim (Henry & Dutrow 1996). Thus we infer a non-detrital origin for the core. However, cores appear to have been resorbed at one stage of the metamorphic evolution (Fig. 11).

SIGNIFICANCE OF OSCILLATORY ZONING DURING GROWTH OF METAMORPHIC MINERALS

The internal zonation in garnet, showing increasing X_{Mg} and grossular content toward the rim, is due to growth of garnet during prograde metamorphism. Related oscillatory zoning in garnet as well as in epidote and tourmaline can also be regarded as a particular growth-induced phenomenon related to continuous pro-

grade reactions. This phenomenon seems to be ubiquitous and independent of the rock type. It was observed in garnet grains within garnet amphibolites from other parts of the Western Series (Willner *et al.* 1999, 2000). Furthermore, similar number of oscillatory cycles were observed in garnet, epidote and tourmaline from different rock-types (greenschists and coticules) of the Bahia Mansa area. This would rather favor a common explanation of the oscillatory zoning. On the other hand, the size of the oscillatory zones around different individual crystals within single samples varies strongly, and oscillatory zoning in garnet was only demonstrable for Ca. Local increase in Ca is not correlated with a decrease of a single other element, but of the sum of the others. These sharp local concentrations probably reflect a local extent of reaction around the individual crystals and differing local availability of material. In any case, these subtle variations reflect very small changes that are mainly detectable by modern imaging techniques.

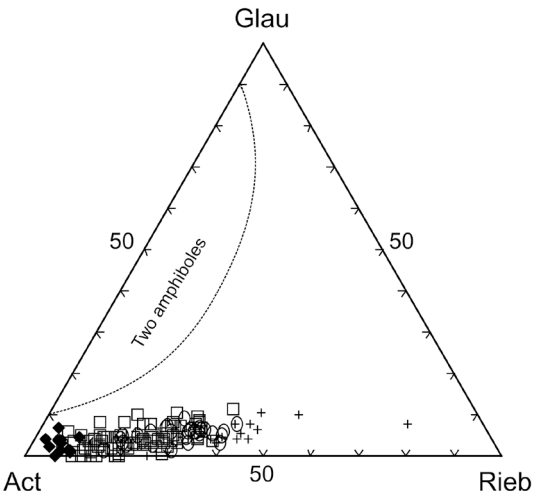

FIG. 10. Variation of amphibole compositions in the system glaucophane – actinolite – riebeckite; $X_{Glau} = (2–Ca)/2 * {}^{VI}Al/({}^{VI}Al + Fe^{3+})$; $X_{Act} = Ca/2$; $X_{Rieb} = 1 – (X_{Glau} + X_{Tr})$; the solvus at 300°C as calculated by Massonne (1995a) is shown.

Three explanations for oscillatory zoning in metamorphic phases have been proposed in the literature: (1) Schumacher *et al.* (1998) have argued that a temporary change of intensive parameters, for instance pressure, could have caused oscillatory zoning. For example, small-scale variation of the subduction velocity could cause a variable slope of the metamorphic path in the P–T field, and therefore favor differences in the rate of production of garnet at different stages. (2) However, as zonation in Ca does not correlate with that in Mn, Mg or Fe^{2+}, relationships as observed by Chernoff & Carlson (1997, 1999) seem conceivable, at least for garnet. According to these authors, Ca and associated trace elements behave anomalously during garnet growth compared to Fe, Mg and Mn owing to a relatively sluggish rate of intergranular diffusion. The concentration of Ca at the surface of the growing crystals probably depends on kinetic factors that govern the local chemical environment. It was shown by Chernoff & Carlson (1997, 1999) that local concentrations of Ca and trace elements were not formed synchronously, as they would

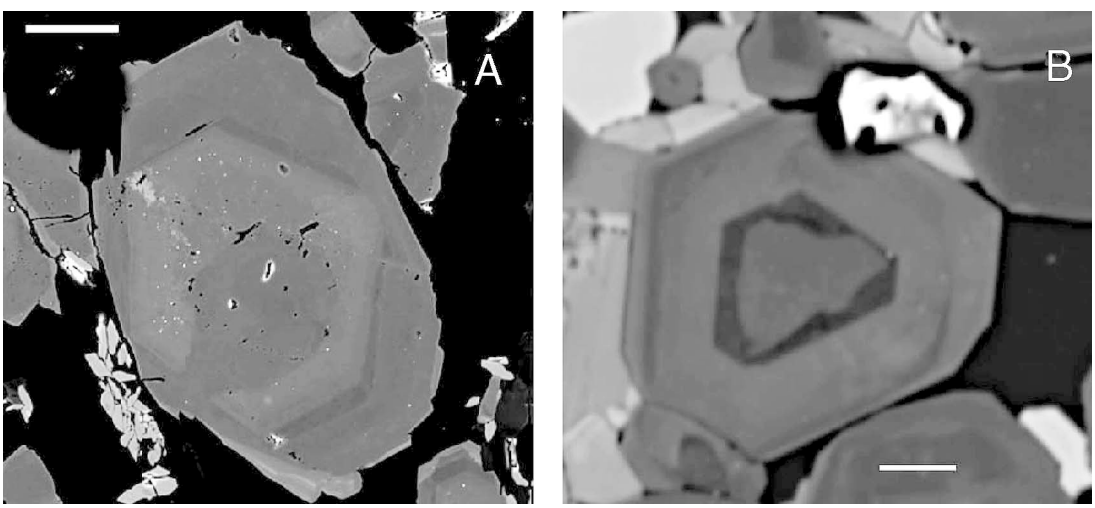

FIG. 11. BSE images of (A) epidote (greenschist sample 96CH–219) and (B) tourmaline (greenschist sample 96CH–214). Scale is 30 μm in (A) and 5 μm in (B).

have during changes in P, T or fluid composition. (3) Furthermore, the two different competing metamorphic fluids (internal and external sources, as will be described below) within the coticules may also have affected the local concentration of Ca. Yardley *et al.* (1991) reported the presence of oscillatory zoning in metamorphic minerals related to non-equilibrium growth in open-system environments. The infiltration of fluid generates supersaturation similarly to the case of minerals grown in hydrothermal systems (Jamtveit *et al.* 1993). Abundant concentrations of epidosite within the greenschists of Bahia Mansa demonstrate the importance of metasomatic processes. However, mineral growth related to such open systems would generate a highly variable and complicated pattern of oscillatory zoning characterized by multiple cycles, not observed in the samples of this study.

We concur with Chernoff & Carlson (1997, 1999) that oscillation may be due to selective flux of elements

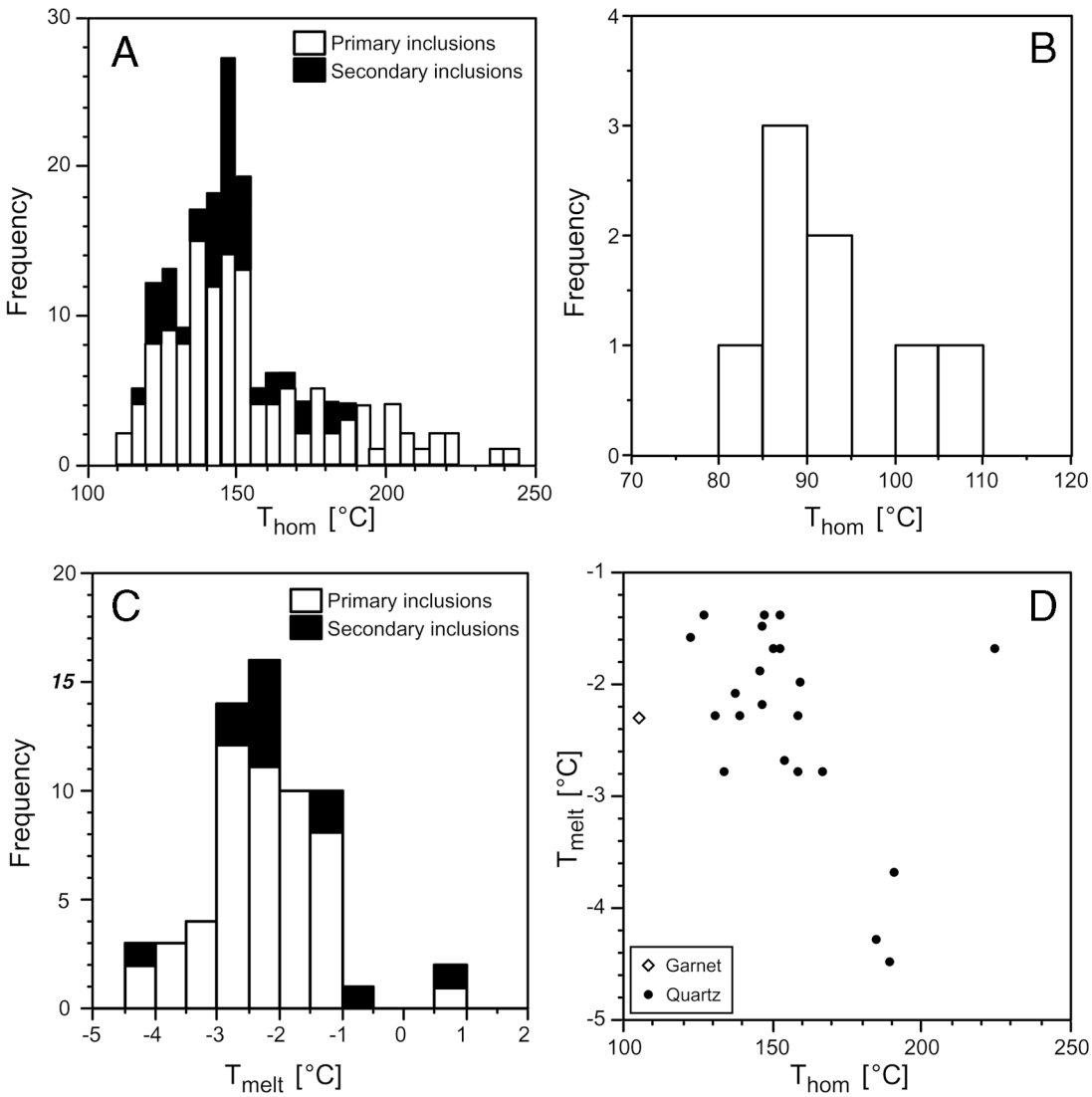

FIG. 12. Histograms showing microthermometric results. Frequency of homogenization temperatures of (A) primary and secondary inclusions in quartz, (B) primary inclusions in garnet, (C) frequency of freezing temperatures in primary and secondary inclusions in quartz, and (D) freezing temperatures *versus* homogenization temperatures for primary inclusions in quartz and garnet.

between reactant and product phases. Certain elements with slow rates of diffusion (*e.g.*, Ca) are temporarily stored in the reactant phases (*e.g.*, carbonates in the coticules) during growth, leading to an element-depletion zone around the product phases (*e.g.*, garnet). Finally, the reactant phase becomes locally unstable and again provides a source of the slow element in response to the decreasing flux of that element toward the product phase.

Fluid Inclusions

Only coticule samples were studied for fluid inclusions. Two generations of fluid inclusions are easily detectable in quartz. Single isolated fluid inclusions, considered to be primary, *i.e.*, formed during recrystallization of their host minerals under peak conditions of metamorphism, were observed in quartz (3–5 μm diameter; gas phase 5–10% of the total volume) and rarely in garnet (2.5 μm; gas phase 5% of the volume). Conspicuous trails of abundant smaller secondary and pseudosecondary inclusions are only present in quartz (2–4 μm diameter; gas phase 5–10% of the volume). All fluid inclusions studied consist of two phases, an aqueous liquid and a vapor bubble. No solid phase was observed. Infrared spectroscopy showed the presence of trace amounts of CO_2 in addition to the predominant H_2O (Lange 1997).

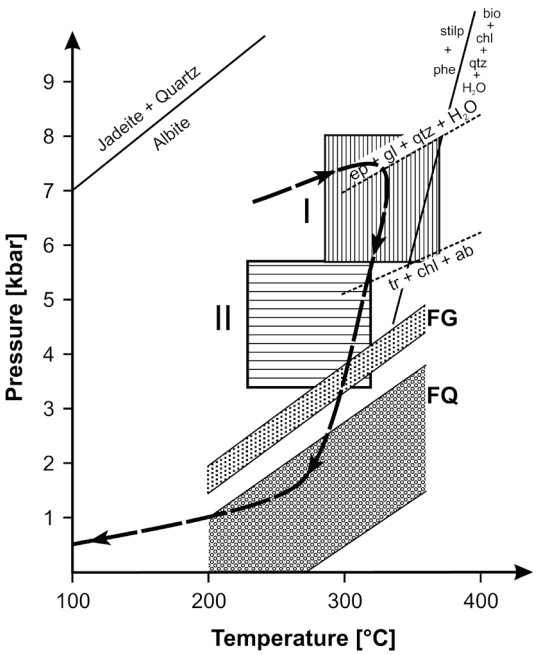

FIG. 13. P–T path for the coticules and adjacent metabasic rocks at Bahia Mansa. The albite-breakdown reaction is taken from Holland (1980), the stilpnomelane + phengite breakdown reaction is from Massonne & Szpurka (1997); multivariant reaction (1) (see text) is calculated for the entire range of compositions at stage I using an activity of H_2O of 1. Box with equilibria at stage I was calculated with reactions (2) – (5) (see text) using maximum Si-compositions in phengite and maximum glaucophane component in NaCa-amphibole. For stage II, compositions with minimum Si-contents of white mica and minimum glaucophane component in actinolite were used. FG corresponds to the range of isochores of primary fluid inclusions in garnet, FQ corresponds to those of primary fluid inclusions in quartz.

Homogenization temperatures for primary and secondary inclusions in quartz are similarly distributed, although they range to higher values for primary inclusions: 113–242°C, mean of 138°C for primary inclusions; 116–188°C, mean of 145°C for secondary inclusions) (Fig.12A). Melting temperatures vary between –1.2 and –4.5°C for both generations (mean: –2.4°C; Fig. 12B) corresponding to relatively low salinities of 2.2–8.9 equiv. wt% NaCl (Bodnar 1993). Homogenization temperatures of fluid inclusions in garnet are between 86.5° and 105°C and thus, significantly lower than those in quartz (Fig. 12C).

Considering the range of homogenization temperature *versus* salinity between 189°C [8.95 wt% (0.88 molal) equiv. NaCl] and 127°C [2.2 wt% (0.42 molal) equiv. NaCl] (Fig. 12D), isochores have been calculated for the aqueous inclusions in quartz using the equation of state for the system H_2O – NaCl (Fig. 13) according to Brown & Lamb (1989). Assuming similar salinities of inclusions in garnet and quartz, the only measured freezing temperature in garnet, –2.3°C (4.2 wt% or 0.83 molal equiv. NaCl), is taken for calculation of all isochores of inclusions in garnet (Fig. 13). Calculated densities in primary inclusions in quartz range from 0.85 to 0.99 g/cm^3, and from 0.98 to 0.99 g/cm^3 for those in garnet. In Figure 13, it becomes apparent that the bundle of isochores passes well below the maximum P–T conditions defined by the mineral equilibria. Furthermore, the range of isochores of primary fluid inclusions in garnet differs significantly from those within quartz.

Phase Relationships and Metamorphic Conditions

The mineral assemblages observed in the metabasic rocks, the amphibole-bearing coticules and the chlorite–amphibole mica schists can be related to a transition between greenschist and epidote-blueschist facies, as defined by Evans (1990). This transition, which occurs between 6 and 9 kbar and between 300 and 500°C, is characterized for instance by the multivariant reactions of following mineral components:

$$\text{clinozoisite}_{ep} + \text{glaucophane}_{amp} + \text{quartz} + H_2O = \text{tremolite}_{amp} + \text{clinochlore}_{chl} + \text{albite}_{pl} \quad (1)$$

TABLE 2. THERMODYNAMIC DATA USED FOR GEOTHERMOBAROMETRY

Component	Mineral	Formula	Data Source	
			End member	Activity formulation
glaucophane	amphibole	$Na_2Mg_3Al_2Si_8O_{22}OH_2$	Evans (1990)	Massonne (1995a, b)
tremolite	amphibole	$Ca_2Mg_5Si_8O_{22}OH_2$	Berman (1988)	Massonne (1995a, b)
clinochlore	chlorite	$Mg_5Al_2Si_3O_{10}OH_8$	Massonne (1995b)	Massonne (1995a)
daphnite	chlorite	$Fe_5Al_2Si_3O_{10}OH_8$	Massonne & Szpurka (1997)	as Massonne (1995a)
clinozoisite	epidote	$Ca_2Al_4Si_3O_{12}OH$	Berman (1988)	$a_{clinozoisite} = 1 - X_{pistacite}$
almandine	garnet	$Fe_3Al_2Si_3O_{12}$	Berman (1990)	Massonne (1995b)
grossular	garnet	$Ca_3Al_2Si_3O_{12}$	Berman (1990)	Massonne (1995b)
pyrope	garnet	$Mg_3Al_2Si_3O_{12}$	Berman (1990)	Massonne (1995b)
albite	plagioclase	$NaAlSi_3O_8$	Berman (1988)	$a_{albite} = X_{albite}$
Fe–Al-celadonite	white mica	$KFeAlSi_4O_{10}OH_2$	Massonne & Szpurka (1997), Massonne (1997)	Massonne (1997)
Mg–Al-celadonite	white mica	$KMgAlSi_4O_{10}OH_2$	Massonne (1995b)	Massonne (1995b, 1997
muscovite	white mica	$KAl_3Si_3O_{10}OH_2$	Massonne (1995b)	Massonne (1995b, 1997
quartz	quartz	SiO_2	Berman (1988)	

The terminology shown here is that utilized in the respective references; note that daphnite, pistacite, Fe–Al-celadonite and Mg–Al-celadonite are not IMA-approved.

and

$$7\ \text{Mg–Al-celadonite}_{wm} + 11\ \text{glaucophane}_{amp} + 6\ \text{clinozoisite}_{ep} + 7\ \text{quartz} = 22\ \text{albite}_{pl} + 2\ \text{clinochlore}_{chl} + 7\ \text{muscovite}_{wm} + 6\ \text{tremolite}_{amp} \quad (2)$$

The Na–Ca amphiboles "ferriwinchite" and "ferribarroisite", which we detected within all rock types studied, could represent index minerals between both facies series dominated by sodic or calcic amphiboles. However, in two greenschist samples (96CH–191, 96CH–196), actinolite is the only amphibole present, but oriented parallel to the same predominant S_2 foliation as the Na–Ca amphiboles in the immediately adjacent samples.

Peak conditions of temperature in the range of 300–350°C are defined by a relatively small P–T field. Spessartine can appear at a temperature as low as 300°C (Theye *et al.* 1996), whereas stilpnomelane + phengite are stable up to 350°C at 6 kbar in the pure KFASH system (Massonne & Szpurka 1997; Fig. 13). This temperature range is also supported by the absence of biotite in all metapsammopelitic rocks of the area and the omnipresent recrystallization of quartz. It can be quantified with conventional Fe–Mg exchange thermometry using Na–Ca amphibole – garnet pairs (Graham & Powell 1984) in coticule samples 96CH–197 and 96CH–201. Correlating rim compositions of garnet (having the highest X_{Mg}) with those of adjacent low-X_{Mg} Na–Ca amphiboles, we find a temperature range of 306°–355°C, marking the thermal peak of metamorphism.

The maximum pressure must have been within the stability field of albite in view of the absence of jadeite. The generally high Si contents of phengite, around 3.3–3.5 *apfu* in all assemblages, points to pressures of 4–7 kbar at 350°C using the revision of the barometer of Massonne & Schreyer (1987) by Massonne (1991). Because K-feldspar is absent, the result is a minimum pressure only.

For a more precise estimate of P–T conditions for various metamorphic stages, we used thermodynamic data of minerals to locate certain mineral equilibria in P–T space. Multivariant metamorphic equilibria were calculated applying the Geø –Calc software package of Brown *et al.* (1989). The data and their sources are recorded in Table 2.

The Na–Ca amphibole with the highest proportion of the glaucophane component, low-Fe epidote (highest proportion of the clinozoisite component) and phengite with the highest Si content (highest proportion of the celadonite component) are considered to have formed at an early metamorphic stage at high pressure (stage I), because those three end-member components occur on the high-pressure side of reactions (1) – (4) and tend to represent the core compositions of the mineral grains. In view of its relatively homogeneous composition, chlorite is not attributed to any particular stage of growth. Reaction (2), involving amphibole, epidote and phengite, provides an ideal barometer for all rock types studied, because it is a H_2O-conserving reaction and thus independent of H_2O activity. It may be combined with the following three H_2O-conserving multivariant reactions of mineral components for thermobarometry, thus defining an invariant point:

$$10\ \text{Fe–Al-celadonite}_{wm} + 11\ \text{glaucophane}_{amp} + 6\ \text{clinozoisite}_{ep} + 7\ \text{quartz} = 22\ \text{albite}_{pl} + 2\ \text{daphnite}_{chl} + 7\ \text{muscovite}_{wm} + 6\ \text{tremolite}_{amp} \quad (3)$$

$$35\ \text{Fe–Al-celadonite}_{wm} + 55\ \text{glaucophane}_{am} + 30\ \text{clinozoisite}_{ep} + 35\ \text{quartz} = 110\ \text{albite}_{pl} + 7\ \text{daphnite}_{chl} + 35\ \text{muscovite}_{wm} + 30\ \text{tremolite}_{am} + 3\ \text{clinochlore}_{chl} \quad (4)$$

and

daphnite$_{chl}$ + 5 Mg–Al-celadonite$_{wm}$
= 5 Fe–Al-celadonite$_{wm}$ + clinochlore$_{chl}$ (5)

Calculations of stage-I conditions result in a scatter of P–T data in the range 265–374°C at 5.9–8.0 kbar (Table 3). The temperatures are compatible with those derived above, suggesting that both the pressure and thermal peak of metamorphism were close together in P–T space. The pressure range also can be confirmed by calculating the white-mica-free reaction (1) assuming an activity of H_2O of unity (Fig. 13). Thus, (1) the metamorphic fluid at peak conditions was essentially hydrous in all samples, (2) P–T conditions at stage I were at least similar in all rocks studied, particularly in those with differing compositions of amphibole at the peak of metamorphism, ranging from Na–Ca amphibole to actinolite (samples 96CH–191, 96CH–196).

It must be noted that pressures calculated using garnet components and the following H_2O-conserving multivariant reaction:

78 clinozoisite$_{ep}$ + 33 tremolite$_{amp}$
= 18 clinochlore$_{chl}$ + 74 grossular$_{grt}$ +
25 pyrope$_{grt}$ + 147 quartz (6)

yielded unreasonably low pressures. We attribute this discrepancy to a poorly (least) known grossular–spessartine solid-solution model and a high Fe^{3+} content in both garnet and coexisting amphibole.

The formation of an actinolite rim around the Na–Ca amphibole, a low-Si rim on white mica, and a high-Fe rim of epidote reflect local retrograde equilibration (stage II). Conditions for stage II can be calculated in the same way as stage I; calculations yield a scatter of P–T data between 3.4 and 5.7 kbar at 230–320°C (Table 3).

TABLE 3. RESULTS OF GEOTHERMOBAROMETRY, METABASIC ROCKS AND COTICULES OF THE BAHIA MANSA COMPLEX, COASTAL CORDILLERA OF CHILE

Sample	Temperature [°C]	Pressure [kbar]	Stage	Method	Rock type
96CH–191	357	8.0	I	1	Metabasic rock
96CH–194	359	(7)	I	1	Metabasic rock
96CH–196	304	6.95	I	1	Metabasic rock
96CH–197	317	7.30	I	1	Coticule
96CH–197	342, 355	(7)	I	2	Coticule
96CH–201	306	(7)	I	2	Coticule
96CH–205	374	8.00	I	1	Metabasic rock
96CH–215	281	6.80	I	1	Metabasic rock
96CH–217	349	7.30	I	1	Metabasic rock
96CH–219	267	5.95	I	1	Metabasic rock
96CH–196	251	5.70	II	1	Metabasic rock
96CH–197	284	3.4	II	1	Coticule
96CH–205	264	5.6	II	1	Metabasic rock
96CH–215	319	5.4	II	1	Metabasic rock
96CH–217	232	3.6	II	1	Metabasic rock

Method 1: calculation of multivariant reactions; method 2: Fe/Mg exchange, garnet/amphibole.

Fluid Evolution During Metamorphism

It has been suggested in some cases that manganese-rich carbonate (rhodochrosite or manganoan siderite) and chlorite are low-T and low-P precursor minerals to coticule assemblages (Schreyer *et al.* 1992, Slack *et al.* 2000). In samples from Bahia Mansa, up to three carbonates were observed coexisting with spessartine-rich garnet, chlorite, quartz and white mica. Hence, various garnet-producing multivariant reactions involving mineral components can be formulated, such as:

18 rhodochrosite$_{carb}$ + clinochlore$_{chl}$ +
5 muscovite$_{wm}$ + 20 quartz
= 5 Mg–Al-celadonite$_{wm}$ +
6 spessartine$_{grt}$ + 4 H_2O + 18 CO_2 (7)

During early growth of garnet, Mn is strongly fractionated into garnet at the expense of Mn components of other solid-solution minerals, particularly carbonates, which afterward become relatively depleted in Mn. Possible original Mn-rich carbonate compositions, found as rhodochrosite inclusions in garnet of the low-grade metapelites in the Ardennes by Schreyer *et al.* (1992), were not detected in samples from Bahia Mansa owing to the small grain-size of the garnet grains. The decarbonation–dehydration reaction should release a mixed internal CO_2–H_2O fluid with a high $X(CO_2)$. However, the nearly pure aqueous fluids trapped in primary inclusions within recrystallized quartz in equilibrium with peak metamorphic phases indicate that the metamorphic fluid was essentially externally buffered. This is obvious, because the bulk of the surrounding rocks are carbonate-free, and the thickness of the coticules is minor. However, this influx of external fluid did not result in a complete breakdown of the carbonates. Growth of secondary carbonate can be excluded in the present case owing to the lack of replacement textures and restriction of carbonates to coticules.

Isochores of primary fluid inclusions in quartz show pressures much below maximum P–T conditions derived from equilibria involving solid phases (Fig. 13). We explain this finding by a continuous reduction of volume owing to stretching during decompression. Using a theoretical approach as well as field observations, Küster & Stöckhert (1997) unambiguously showed that small differential pressures (difference between internal fluid pressure and external lithostatic pressure) cause widening of inclusions in quartz within high-pressure rocks, whereas pressure changes considerably during decompression above 300°C, as induced by dislocation creep. Good arguments for this process in the coticules studied are (1) significantly higher densities in inclusions within garnet as a mineral with much higher flow strength than quartz (also shown with aragonite *versus* quartz by Küster & Stöckhert 1997), and (2) similar densities of primary and secondary inclusions in quartz. The observed densities of the fluid

became fixed during cooling below 300°C, when dislocation creep ceases in quartz. Hence the resulting isochores for primary inclusions in quartz give a valuable indicator of retrograde pressure near that "closure" temperature of 300°C, which is also a further constraint on the P–T path (Fig. 13): The early retrograde P–T path derived is the result of decompression with slight cooling followed by a marked kink at low pressures around 2 kbar.

Conclusions

Considering the abundant occurrence of other rocks of exhalative origin in the broader context of the study area (iron formation, massive sulfide, tourmalinite), as well as many features of the distribution of major and trace elements, the spessartine quartzites of Bahia are comparable to many occurrences of coticules worldwide. However, they differ from most occurrences (1) by their association with dismembered ophiolites, *i.e.*, oceanic crust incorporated into an accretionary prism, and (2) by their high SiO_2 content, marking the upper end of the range of coticule compositions. We suggest that their protolith was a mixture of hydrothermal ferroan and manganiferous precipitates and concomitantly formed aluminous restite material originating by alteration of pelagic sediments and tuffs. Carbonates were important precursor phases that are still in mutual contact with garnet in the present rocks. They were involved in continuous dehydration–decarbonation reactions at conditions of peak metamorphism to form garnet. Strong similarity of the minerals in all three rock types studied with respect to major-element composition and the bulk concentration of some trace elements such as Ba points to a common premetamorphic origin as well as to a common metamorphic evolution.

The peak P–T conditions of metamorphism suggest a metamorphic gradient of around 12°C/km that (1) seems to characterize much of the Western Series of the basement in central and southern Chile (Willner *et al.* 1999, 2000), and (2) is also evident in models of evolution of accretionary prisms during slow subduction, according to the numerical experiments of Peacock (1996). The peak conditions of metamorphism are related to the transition from the greenschist to the epidote blueschist facies. Thus the different compositions of amphibole that we observed in similar mineral assemblages can be explained. Greenschist-facies assemblages also formed at high-P and low-T conditions, as did rocks containing Na–Ca amphibole and phengite that constitute true transitional assemblages toward blueschist facies, reflecting high Fe^{3+} contents of the protolith rock-types. All visible penetrative ductile deformation occurred at high-pressure conditions.

The retrograde P–T path is characterized by (1) strong decompression with slight cooling, with external influx of fluid presumably owing to concomitant subduction of material undergoing prograde dehydration, and finally by strain-free crystallization of retrograde phases, and (2) a kink toward cooling with slight decompression at low pressures. A complete retrograde overprint was not observed.

Acknowledgements

This research was supported by the German–Chilean BMBF–CONICYT cooperation project Chl 01A 6A "High pressure metamorphic rocks in Chile". We thank J. Muñoz (SERNAGEOMIN Puerto Varas) for logistical support during a field trip to Bahia Mansa in 1996, B. Schulz-Dobrick for providing analytical facilities at the University of Mainz, and S. Chakraborty for advice on the manuscript. The paper was substantially improved by thorough reviews by P. Spry and J. Thompson as well as careful editorial handling by R.F. Martin. This study is also a contribution to IGCP 436 "Pacific Gondwana Margin".

References

Aguirre, L., Hervé, F. & Godoy, E. (1972): Distribution of metamorphic facies in Chile: an outline. *Krystallinikum* **9**, 7-19.

Berman, R.G. (1988): Internally-consistent thermodynamic data for minerals in the system Na_2O–K_2O–CaO–MgO–FeO–Fe_2O_3–Al_2O_3–SiO_2–TiO_2–H_2O–CO_2. J. *Petrol.* **29**, 445-522.

_____ (1990): Mixing properties of Ca–Mg–Fe–Mn garnets. *Am. Mineral.* **75**, 328-344.

Bjerkgard, T. & Bjorlykke, A. (1996): Sulfide deposits in Folldal, southern Trondheim Region Caledonides, Norway: source of metals and wall rock alterations related to host rocks. *Econ. Geol.* **91**, 676-696.

Bodnar, R.J. (1993): Revised equation and table for determining the freezing point depression of H_2O–NaCl solutions. *Geochim. Cosmochim. Acta* **57**, 683-684.

Bonatti, E. (1975): Metallogenesis at oceanic spreading centers. *Annu. Rev. Earth Planet. Sci.* **3**, 401-431.

Brimhall, G.H. & Crerar, D.A. (1987): Ore fluids: magmatic to supergene. *In* Thermodynamic Modeling of Geological Materials: Minerals, Fluids and Melts (I.S.E. Carmichael & H.P. Eugster, eds.). *Rev. Mineral.* **17**, 235-321.

Brown, P.E. & Lamb, W.M. (1989): P–V–T properties of fluids in the system $H_2O \pm CO_2 \pm$ NaCl: new graphical presentations and implications for fluid inclusion studies. *Geochim. Cosmochim. Acta* **53**, 1209-1221.

Brown, T.H., Berman, R.G. & Perkins, E.H. (1989): GEØ-CALC: software package for calculation and display of pressure – temperature – composition phase diagrams using an IBM or compatible personal computer. *Comput. Geosci.* **14**, 279-289.

CHERNOFF, C.B. & CARLSON, W.D. (1997): Disequilibrium for Ca during growth of pelitic garnet. *J. Metamorph. Geol.* **15**, 421-438.

_____ & _____ (1999): Trace element zoning as a record of chemical disequilibrium during garnet growth. *Geology* **27**, 555-558.

COLLAO, S., ALFARO, G. & HAYASHI, K. (1990): Banded iron formation and massive sulfide ore bodies, south-central Chile: geological and isotopic aspects. *In* Stratabound Ore Deposits in the Andes (L. Fontboté, G.C. Amstutz, M. Cardozo, E. Cedillo & J. Frutos, eds.). Springer, Heidelberg, Germany (209-219).

_____, KOJIMA, S. & OYARZUN, R. (1986): Geobarometria en los sulfuros macizos de la franja metamorfica de esquistos verdes, Chile central-sur. *Rev.Geol.Chile* **28/29**, 3-16.

DUHART, P., MARTIN, M.W., MUNOZ, J., CRIGNOLA, P. & MCDONOUGH, M. (1997): Acerca de la edad del protolito de basamento metmórfico de la Cordillera de la Costa de la X region: edades preliminares $^{207}Pb/^{206}Pb$ en circones detríticos. *8. Congreso Geológico Chileno* (*Antofagasta*), 1267-1270.

EL SHAZLY, A., COLEMAN, R.G. & LIOU, J.G. (1990): Eclogites and blueschists from northeastern Oman: petrology and PT-evolution. *J. Petrol.* **31**, 629-666.

EVANS, B.W. (1990): Phase relations of epidote-blueschists. *Lithos* **25**, 3-23.

GRAHAM, C.M. & POWELL, R. (1984): A garnet–hornblende geothermometer and application to the Peloma Schist, southern California. *J. Metamorph. Geol.* **2**, 13-32.

HENRY, D.J. & DUTROW, B.J. (1996): Metamorphic tourmaline and its petrologic applications. *In* Boron – Mineralogy, Petrology and Geochemistry (E.S. Grew & L.M. Anovitz, eds.). *Rev. Mineral.* **33**, 503-558.

HERVÉ, F. (1988): Late Paleozoic subduction and accretion in southern Chile. *Episodes* **11**, 183-188.

HOLLAND, T.J.B. (1980): The reaction albite = jadeite + quartz determined experimentally in the range 600–1200°C. *Am. Mineral.* **65**, 129-134.

JAMTVEIT, B., WOGELIUS, R.A. & FRASER, D.G. (1993): Zonation patterns of skarn garnets: records of hydrothermal system evolution. *Geology* **21**, 113-116.

KATO, T.T. (1985): Pre-Andean orogenesis in the Coast Ranges of central Chile. *Geol. Soc. Am., Bull.* **96**, 918-924.

_____ & GODOY, E. (1995): Petrogenesis and tectonic significance of Late Paleozoic coarse-crystalline blueschist and amphibolite boulders in the coastal range of Chile. *Int. Geol. Rev.* **37**, 992-1006.

_____, _____, MCDONOUGH, M., DUHART, P., MARTIN, M.W. & SHARP, W. (1997): Un modelo preliminar de deformación transpresional Mesozoica y gran desplazamiento hacia el Norte de parte de la Serie Occidental, Complejo Acrecionario (38ºS a 43ºS), Cordillera de la Costa, Chile. *8. Congreso Geológico Chileno* (*Antofagasta*), 98-102.

KRAMM, U. (1976): The coticule rocks (spessartine quartzites) of the Venn–Stavelot Massif, Ardennes, a volcanoclastic metasediment? *Contrib. Mineral. Petrol.* **56**, 135-155.

KRETZ, R. (1983): Symbols for rock forming minerals. *Am. Mineral.* **68**, 277-279.

KROSSE, S. & SCHREYER, W. (1993): Comparative geochemistry of coticules (spessartine-quartzites) and their redschist country rocks in the Ordovician of the Ardennes Mountains, Belgium. *Chem. Erde* **53**, 1-20.

KÜSTER, M. & STÖCKHERT, B. (1997): Density changes of fluid inclusions in high-pressure low-temperature metamorphic rocks from Crete: a thermobarometric approach based on the creep strength of host minerals. *Lithos* **41**, 151-167.

LANGE, S. (1997): Metamorphite eines Akkretionskomplexes im jungpaläozoischen Grundgebirge bei Bahia Mansa, südliches Zentralchile. *Diploma thesis, Univ. Mainz, Mainz, Germany*.

LEAKE, B.E. and 21 others (1997): Nomenclature of amphiboles. Report of the subcommittee on amphiboles of the International Mineralogical Association Commision on New Minerals and Mineral Names. *Eur. J. Mineral.* **9**, 623-651.

MARTIN, M.W., KATO, T.T., RODRIGUEZ, C., GODOY, E., DUHART, P., MCDONOUGH, M. & CAMPOS, A. (1999): Evolution of the late Paleozoic accretionary complex and overlying forearc – magmatic arc, south central Chile (38º–41ºS): constraints for the tectonic setting along the southwestern margin of Gondwana. *Tectonics* **18**, 582-605.

MARUYAMA, S. & LIOU, J.G. (1988): Petrology of Franciscan metabasites along the jadeite–glaucophane type facies series, Cazadero, California. *J. Petrol.* **29**, 1-37.

MASSONNE, H.-J. (1991): *High-Pressure, Low-Temperature Metamorphism of Pelitic and other Protoliths Based on Experiments in the System K_2O–MgO–Al_2O_3–SiO_2–H_2O*. Thesis of habilitation, Univ. Bochum, Bochum, Germany.

_____ (1995a): P–T evolution of metavolcanics from the southern Taunus mountains. *In* Pre-Permian Geology of Central and Eastern Europe (R.D. Dallmeyer, W. Franke & W. Weber, eds.). Springer Verlag, Berlin, Germany (132-137).

_____ (1995b): Experimental and petrogenetic study of UHPM. *In* Ultrahigh Pressure Metamorphism (R.G. Coleman & X. Wang, eds.). Cambridge University Press, Cambridge, U.K. (33-95).

_____ (1997): An improved thermodynamic solid solution model for natural white micas and its application to the geothermobarometry of metamorphic rocks. *In* Mineral

Equilibria and Databases. *Geol. Surv. Finland, Guide* **46**, 49 (abstr.).

_____, HERVÉ, F., MEDENBACH, O., MUNOZ, V. & WILLNER, A.P. (1998): Zussmanite in ferrugineous metasediments from southern central Chile. *Mineral. Mag.* **62**, 869-876.

_____, _____, MUNOZ, V. & WILLNER, A.P. (1996): New petrological results on high-pressure, low-temperature metamorphism of the Upper Paleozoic basement of central Chile. *Third Int. Symp. on Andean Geodynamics* (*St. Malo*), 783-785 (abstr.).

_____ & SCHREYER, W. (1987): Phengite geobarometry based on the limiting assemblage with K-feldspar, phlogopite and quartz. *Contrib. Mineral. Petrol.* **96**, 212-224.

_____ & SZPURKA, Z. (1997): Thermodynamic properties of white micas on the basis of high-pressure experiments in the systems K_2O–MgO–Al_2O_3–SiO_2–H_2O and K_2O–FeO–Al_2O_3–SiO_2–H_2O. *Lithos* **41**, 229-250.

MUÑOZ, V. & HERVÉ, F. (2000): Concideraciones de alta presion – baja temperatura para la serie oeste del basamento metamorfico paleozoico, en base a clorita, cimrita y mica blanca en sulfuros masivos de Piren Alto. *Actas IX. Congreso Chileno de Geología* **1**, 654-658.

PEACOCK, S.M. (1996): Thermal and petrologic structure of subduction zones. *In* Subduction – Top to Bottom (G.E. Behout, D.W. Scholl, S.H. Kirby & J. Platt, eds.). *Am. Geophys. Union, Geophys. Monogr.* **96**, 119-131.

RENARD, A. (1878): Sur la structure et la composition minéralogique du coticule et sur ses rapports avec le phyllade oligistifère. *Acad. Royale Belgique, Mém.* **41**.

ROSENBERG, P.E. (1963): Subsolidus relations in the system $CaCO_3$–$FeCO_3$. *Am. J. Sci.* **261**, 683-690.

SCHIRA, W., AMSTUTZ, G.C. & FONTBOTÉ, L. (1990): The Pirén Alto Cu–(Zn) massive sulfide occurrence in south-central Chile – a kieslager-type mineralization in a Paleozoic ensialic mature marginal basin setting. *In* Stratabound Ore Deposits in the Andes (L. Fontboté, G.C. Amstutz, M. Cardozo, E. Cedillo & J. Frutos, eds.). Springer, Heidelberg, Germany (229-251).

SCHREYER, W., BERNHARDT, H.J. & MEDENBACH, O. (1992): Petrologic evidence for a rhodochrosite precursor of spessartine in coticules of the Venn–Stavelot massif, Belgium. *Mineral. Mag.* **56**, 527-532.

SCHUMACHER, R., RÖTZLER, K. & MARESCH, W.V. (1998): Subtle oscillatory zoning in garnet from regional metamorphic phyllites and mica schists, western Erzgebirge, Germany. *Can. Mineral.* **37**, 381-402.

SLACK, J.F., SHAW, D.R., LEITCH, C.H.B. & TURNER, R.J.W. (2000): Tourmalinites and coticules from the Sullivan Pb–Zn–Ag deposit and vicinity, British Columbia: geology, geochemistry and genesis. *In* Geological Environment of the Sullivan Deposit, British Columbia (J.W. Lydon, T. Höy, J.F. Slack & M.E. Knapp, eds.). *Geol. Assoc. Can., Spec. Vol.* (in press).

SOKOLOVA, E.V., HAWTHORNE, F.C., GORBATOVA, V., MCCAMMON, C. & SCHNEIDER, J. (2001): Ferrian winchite from the Ilmen Mountains, southern Urals, Russia, and some problems with the current scheme for amphibole nomenclature. *Can. Mineral.* **39**, 171-177.

SPRY, P.G. (1990): Geochemistry and origin of coticules (spessartine–quartz rocks) associated with metamorphosed massive sulfide deposits. *In* Regional Metamorphism of Ore Deposits (P.G. Spry & L.L. Bryndzia, eds.). VSP, Utrecht, The Netherlands (49-75).

_____, PETERS, J. & SLACK, J.F. (2000): Meta-exhalites as keys in the search for metamorphosed ore deposits. *In* Metamorphosed and Metamorphogenic Ore Deposits (P.G. Spry, B. Marshall & F.M. Vokes, eds.). *Rev. Econ. Geol.* **11**, 163-201.

_____ & WONDER, J.D. (1989): Manganese-rich rocks associated with the Broken Hill lead–zinc–silver deposit, New South Wales, Australia. *Can. Mineral.* **27**, 275-292.

THEYE, T., SCHREYER, W. & FRANSOLET, A.M. (1996): Low-temperature, low-pressure metamorphism of Mn-rich rocks in the Lienne Syncline, Venn-Stavelot massif (Belgian Ardennes), and the role of carpholite. *J. Petrol.* **37**, 767-783.

WILLNER, A.P., HERVÉ, F. & MASSONNE, H.-J. (2000): Mineral chemistry and pressure–temperature evolution of two contrasting high-pressure – low-temperature belts in the Chonos Archipelago, southern Chile. *J. Petrol.* **41**, 309-330.

_____, MASSONNE, H.-J. & HERVÉ, F. (1999): Comparison of the PTd-evolution of HP/LT metamorphic rocks in the South Shetland Islands and along the Coastal Cordillera of Chile. *8th Int. Symp. Antarct. Earth Sci.* (*Wellington*), *Abstr. Vol.*, 320.

WONDER, J.D., SPRY, P.G. & WINDOM, K.E. (1988): Geochemistry and origin of manganese-rich rocks related to iron formation and sulfide deposits, western Georgia. *Econ. Geol.* **83**, 1070-1081.

YARDLEY, B.W.D., ROCHELLE, C.A., BARNICOAT, A.C. & LLOYD, G.E. (1991): Oscillatory zoning in metamorphic minerals: an indicator of infiltration metasomatism. *Mineral. Mag.* **55**, 357-365.

Received March 31, 2001, revised manuscript accepted October 15, 2001.

APPENDICES. TABLES OF ANALYTICAL DATA

TABLE A1. COMPOSITION OF GARNET, BAHIA MANSA, CHILE

Sample	96CH-197a Core	96CH-197a Rim	96CH-197b Core	96CH-197b Rim	96CH-201 Core	96CH-201 Rim
SiO_2 wt%	36.59	37.37	36.43	36.96	36.96	37.34
TiO_2	0.24	0.08	0.27	0.20	0.25	0.10
Al_2O_3	18.68	20.31	17.72	20.03	18.86	19.11
Cr_2O_3	0.06	0.08	0.05	0.01	0.00	0.03
FeO	2.05	13.41	1.83	10.84	3.11	8.57
Fe_2O_3*	3.05	1.11	4.80	1.84	2.86	2.89
MnO	31.16	19.95	30.73	23.02	29.71	23.95
MgO	0.07	0.43	0.07	0.37	0.10	0.35
CaO	7.81	7.88	8.45	7.66	8.00	8.26
Sum	99.71	100.62	100.35	100.93	99.85	100.71
Si *apfu*	5.986	6.002	5.956	5.950	6.017	6.023
^{IV}Al	0.014	0.000	0.044	0.050	0.000	0.000
^{VI}Al	3.587	3.845	3.369	3.751	3.619	3.633
Cr	0.008	0.011	0.006	0.001	0.000	0.003
Fe^{3+}	0.376	0.135	0.591	0.223	0.351	0.351
Ti	0.030	0.010	0.033	0.025	0.031	0.013
Mg	0.016	0.102	0.016	0.088	0.024	0.084
Fe^{2+}	0.280	1.801	0.250	1.459	0.424	1.156
Mn	4.317	2.714	4.255	3.139	4.096	3.272
Ca	1.369	1.356	1.480	1.321	1.395	1.427
X_{Alm}	0.047	0.301	0.042	0.243	0.071	0.195
X_{And}	0.094	0.034	0.148	0.056	0.088	0.088
X_{Grs}	0.126	0.188	0.089	0.158	0.139	0.152
X_{Sps}	0.722	0.454	0.709	0.522	0.690	0.551
X_{Prp}	0.003	0.017	0.003	0.015	0.004	0.014

* Cations based on 48 valences, including 10 cations in the tetrahedral and octahedral sites, to calculate proportion of Fe^{3+}. Symbols of garnet components after Kretz (1983).

TABLE A2. COMPOSITION OF CARBONATE, BAHIA MANSA, CHILE

Sample	96CH-197a	96CH-197b	96CH-197c	96CH-201	96CH-201
Na_2O wt%	0.03	0.00	0.03	0.00	0.02
K_2O	0.05	0.04	0.04	0.11	0.01
SrO	0.41	0.00	0.07	0.09	0.04
BaO	0.38	0.07	0.00	0.04	0.02
MgO	18.16	0.22	0.91	0.24	0.14
CaO	33.00	5.51	57.67	56.93	4.60
MnO	0.13	14.73	1.38	4.89	11.16
FeO	4.75	40.95	3.05	0.81	44.01
Sum	56.91	61.52	63.15	63.11	60.00
Na *apfu*	0.005	0.000	0.004	0.000	0.003
K	0.005	0.005	0.004	0.013	0.001
Sr	0.021	0.000	0.004	0.004	0.002
Ba	0.014	0.003	0.000	0.002	0.001
Mg	2.420	0.037	0.124	0.033	0.024
Ca	3.166	0.668	5.541	5.482	0.575
Mn	0.010	1.412	0.102	0.373	1.102
Fe^{2+}	0.356	3.876	0.226	0.061	4.294
X_{Cal}	0.528	0.111	0.923	0.914	0.096
X_{Rd}	0.059	0.646	0.038	0.010	0.716
X_{Mgs}	0.403	0.006	0.021	0.005	0.004
X_{Rds}	0.002	0.235	0.017	0.063	0.184

Symbols of carbonate components after Kretz (1983), except for Mgs, magnesite.

TABLE A3. COMPOSITION OF TOURMALINE, BAHIA MANSA, CHILE

SiO_2 wt%	36.66	36.43	Si *apfu*	6.000	6.000
TiO_2	0.19	0.30	Al	5.733	5.755
Al_2O_3	29.72	29.65			
Cr_2O_3	0.01	0.00	Ti	0.023	0.037
FeO	10.29	10.03	Cr	0.001	0.000
MnO	0.14	0.10	Fe	1.408	1.381
MgO	6.18	6.14	Mn	0.020	0.013
CaO	0.10	0.14	Mg	1.507	1.507
BaO	0.00	0.00			
Na_2O	2.82	2.76	Ca	0.017	0.025
K_2O	0.03	0.02	Ba	0.000	0.000
Cl	0.00	0.01	Na	0.895	0.881
F	0.05	0.00	K	0.007	0.005
H_2O*	3.64	3.64			
B_2O_3**	10.62	10.55	Cl	0.000	0.001
			F	0.026	0.000
Sum***	100.43	99.77	OH	3.974	3.999
			B	3.000	3.000

The proportion of cations is based on 58 valences, B = 3 *apfu*, and F + Cl + OH = 4. * H_2O and ** B_2O_3 calculated. *** The sum is corrected for F and Cl. Both compositions pertain to tourmaline in sample 96CH-214.

TABLE A4. COMPOSITION OF STILPNOMELANE, BAHIA MANSA, CHILE

Sample	96CH-197	96CH-201		96CH-197	96CH-201
SiO_2 wt%	46.13	47.76	Si *apfu*	7.903	8.002
TiO_2	0.01	0.01	^{IV}Al	1.097	0.998
Al_2O_3	5.82	6.10			
Cr_2O_3	0.07	0.00	^{VI}Al	0.079	0.206
FeO	23.21	22.01	Cr	0.009	0.000
MnO	5.34	5.19	Ti	0.001	0.001
MgO	7.09	7.90	Fe^{2+}	2.958	2.983
BaO	0.20	0.96	Fe^{3+}	0.367	0.100
CaO	0.00	0.01	Mn	0.775	0.736
Na_2O	0.67	0.56	Mg	1.810	1.973
K_2O	4.48	2.34			
F	0.03	0.01	Ca	0.000	0.002
H_2O*	5.24	5.36	Ba	0.014	0.063
			Na	0.223	0.183
Sum**	98.56	98.29	K	0.979	0.500
			Total	1.215	0.748
			F	0.014	0.007
			OH	5.986	5.993

The proportion of cations is based on 47.375 valences, neglecting K + Na. The proportion of Fe^{3+} is estimated assuming 15 cations; OH + F = 6. * The proportion of H_2O is calculated. ** The sum is corrected for F.

TABLE A5. COMPOSITION OF TITANITE, BAHIA MANSA, CHILE

Sample	96CH-192	96CH-205	96CH-215		96CH-192	96CH-205	96CH-215
SiO_2 wt%	30.43	30.66	30.94	Si *apfu*	0.996	0.999	1.005
TiO_2	38.21	38.94	34.86				
Al_2O_3	1.48	1.10	2.91	Ti	0.940	0.954	0.852
Fe_2O_3	0.24	0.89	1.35	Al	0.057	0.042	0.111
Mn_2O_3	0.07	0.13	0.03	Fe^{3+}	0.006	0.022	0.033
MgO	0.01	0.00	0.03	Mn^{3+}	0.002	0.003	0.001
CaO	28.49	28.10	28.64	Mg	0.001	0.000	0.001
F	0.49	0.45	0.68	Total	1.006	1.021	0.998
H_2O*	0.06	0.08	0.35				
				Ca	0.999	0.981	0.997
Sum**	99.34	100.28	99.63				
				F	0.047	0.043	0.065
				OH	0.012	0.018	0.075
				O	4.938	4.954	4.859
				Total	4.997	5.015	4.999

Sum of cations: 3; OH = (Al + Fe^{3+}) – F. * The amount of H_2O is calculated. The amount of O = [(Σ positive valences) – OH – F] / 2. ** The sum is corrected for the amount of F. The amount of Cl is below the detection limit.

TABLE A6. COMPOSITION OF CHLORITE, BAHIA MANSA, CHILE

Sample	96CH-191	96CH-192	96CH-194	96CH-196	96CH-197	96CH-201	96CH-205	96CH-215	96CH-217	96CH-219
SiO_2 wt%	26.32	25.50	25.77	26.84	26.80	26.06	26.63	27.46	26.89	27.29
Al_2O_3	19.75	21.15	20.01	19.43	18.94	18.78	18.88	17.96	18.97	19.15
MgO	13.66	12.49	12.91	15.30	15.62	14.63	15.12	17.90	18.12	19.44
FeO	28.09	28.59	27.60	25.28	25.24	27.10	26.69	22.49	22.58	21.70
MnO	0.26	0.28	0.33	0.43	1.27	1.27	0.73	0.81	0.57	0.34
TiO_2	0.01	0.04	0.03	0.09	0.03	0.00	0.01	0.00	0.01	0.05
F	0.00	0.00	0.00	0.00	0.06	0.00	0.00	0.07	0.08	0.11
Cl	0.01	0.00	0.03	0.00	0.00	0.00	0.02	0.01	0.04	0.01
H_2O*	11.28	11.25	11.11	11.36	11.33	11.22	11.32	11.35	11.41	11.60
Sum**	99.53	99.50	98.08	98.91	99.34	99.25	99.52	98.12	98.74	99.72
Si *apfu*	5.594	5.436	5.560	5.668	5.658	5.571	5.640	5.755	5.628	5.619
^{IV}Al	2.406	2.564	2.440	2.332	2.342	2.429	2.360	2.215	2.372	2.381
^{VI}Al	2.541	2.749	2.648	2.503	2.371	2.303	2.353	2.244	2.308	2.266
Ti	0.002	0.007	0.005	0.015	0.005	0.000	0.002	0.000	0.002	0.007
Fe^{2+}	4.992	5.096	4.980	4.464	4.456	4.845	4.727	3.962	3.952	3.736
Mn	0.047	0.051	0.060	0.076	0.227	0.230	0.130	0.145	0.101	0.059
Mg	4.327	3.968	4.151	4.815	4.915	4.662	4.773	5.620	5.653	5.966
F	0.000	0.000	0.000	0.000	0.042	0.000	0.000	0.049	0.055	0.072
Cl	0.004	0.000	0.012	0.000	0.000	0.000	0.009	0.003	0.013	0.002
OH	15.996	16.000	15.988	16.000	15.958	16.000	15.991	15.947	15.932	15.926

The proportion of cations is based on 56 valences. * The amount of H_2O is calculated. ** The sum is corrected for F and Cl; F + Cl + OH = 16.

TABLE A7. COMPOSITION OF EPIDOTE, BAHIA MANSA, CHILE

Sample	96CH-191	96CH-194	96CH-196	96CH-196	96CH-197	96CH-197	96CH-205	96CH-205	96CH-215	96CH-215	96CH-217	96CH-217	96CH-219
Stage	I	I	II	I	I	II	II	I	II	I	I	II	I
SiO_2 wt%	39.58	38.30	37.58	38.15	37.50	37.40	37.40	37.78	37.03	37.81	37.86	37.34	37.73
TiO_2	0.08	0.10	0.18	0.09	0.08	0.05	0.07	0.05	0.08	0.06	0.04	0.01	0.15
Al_2O_3	24.90	24.71	22.46	25.20	21.39	21.57	21.86	22.59	21.26	23.40	23.52	22.18	24.18
Cr_2O_3	0.02	0.01	0.00	0.04	0.02	0.01	0.02	0.02	0.01	0.00	0.00	0.00	0.09
Fe_2O_3	8.80	10.49	14.31	10.86	15.01	15.60	15.61	13.66	15.29	12.94	13.22	14.81	12.18
Mn_2O_3	0.28	0.09	0.00	0.22	0.88	0.99	0.77	0.68	0.72	0.42	0.48	0.43	0.23
MgO	0.89	003	0.01	0.00	0.02	0.03	0.02	0.02	0.01	0.00	0.02	0.00	0.01
CaO	22.74	23.50	23.17	23.56	23.15	21.67	21.94	22.35	21.99	22.71	23.13	23.12	22.92
Na_2O	0.19	0.01	0.00	0.00	0.02	0.01	0.00	0.00	0.00	0.01	0.02	0.01	0.09
H_2O*	3.96	3.83	3.72	3.81	3.72	3.65	3.73	3.77	3.70	3.77	3.78	3.73	3.76
Sum	101.43	101.07	101.47	101.93	101.07	100.70	101.42	100.92	100.10	101.12	102.07	101.64	101.34
Si *apfu*	3.000	3.000	3.000	3.000	3.000	3.000	3.000	3.000	3.000	3.000	3.000	3.000	3.000
Al	2.224	2.281	2.113	2.335	2.017	2.059	2.067	2.114	2.030	2.188	2.197	2.100	2.266
Cr	0.001	0.000	0.000	0.002	0.001	0.001	0.001	0.001	0.001	0.000	0.000	0.000	0.006
Fe^{3+}	0.502	0.618	0.860	0.642	0.904	0.951	0.942	0.816	0.922	0.772	0.789	0.896	0.729
Mn^{3+}	0.016	0.006	0.000	0.013	0.066	0.061	0.047	0.041	0.044	0.025	0.029	0.026	0.014
Mg	0.100	0.003	0.001	0.000	0.003	0.004	0.002	0.002	0.001	0.000	0.002	0.000	0.001
Ti	0.004	0.006	0.011	0.005	0.005	0.003	0.005	0.003	0.005	0.004	0.003	0.001	0.009
Ca	1.846	1.972	1.982	1.985	1.984	1.880	1.886	1.901	1.909	1.931	1.964	1.990	1.953
Na	0.028	0.001	0.000	0.000	0.003	0.003	0.000	0.000	0.000	0.002	0.003	0.002	0.014
OH	2.000	2.000	2.000	2.000	2.000	2.000	2.000	2.000	2.000	2.000	2.000	2.000	2.000
$X_{Pistacite}$	0.502	0.614	0.860	0.643	0.904	0.951	0.942	0.816	0.932	0.772	0.789	0.896	0.729

The proportion of cations is based on a total of three atoms of Si. * The amount of H_2O is calculated on the basis of OH = 2; F + Cl below detection limit. "Pistacite" refers to a hypothetical ferric-iron end-member of epidote.

TABLE A8. COMPOSITION OF PHENGITE, BAHIA MANSA, CHILE

Sample	96CH-191	96CH-192	96CH-194	96CH-196	96CH-196	96CH-197	96CH-197	96CH-205	96CH-205	96CH-215	96CH-215	96CH-217	96CH-217	96CH-219
Stage	I	I	I	I	II	I	II	I	II	I	II	I	II	I
SiO_2 wt%	50.95	50.23	50.68	49.36	47.73	47.46	46.88	47.68	47.02	51.16	46.82	49.26	47.70	51.52
TiO_2	0.07	0.22	0.08	0.13	0.30	0.28	0.44	0.30	0.35	0.07	0.20	0.12	0.22	0.11
Al_2O_3	25.39	27.12	25.83	25.34	26.13	24.88	25.38	24.82	26.03	23.59	22.75	24.69	24.17	24.19
Cr_2O_3	0.08	0.05	0.00	0.00	0.00	0.00	0.00	0.00	0.00	0.00	0.03	0.03	0.09	0.07
FeO	3.24	3.37	3.09	3.69	5.12	5.32	6.20	6.57	5.21	4.09	9.72	4.87	6.98	3.25
MnO	0.01	0.11	0.06	0.01	0.00	0.05	0.08	0.00	0.06	0.01	0.03	0.01	0.05	0.06
MgO	3.28	2.62	2.98	3.40	2.83	2.97	2.79	2.88	2.89	3.94	3.53	3.19	2.89	4.14
CaO	0.00	0.00	0.00	0.00	0.00	0.02	0.00	0.00	0.00	0.01	0.05	0.02	0.02	0.00
BaO	0.22	0.18	0.60	2.36	2.73	2.67	2.39	1.70	3.76	0.58	0.72	0.61	0.42	0.78
Na_2O	0.21	0.33	0.27	0.24	0.31	0.39	0.35	0.33	0.38	0.09	0.19	0.22	0.27	0.19
K_2O	10.99	10.09	10.84	9.89	9.91	9.97	9.95	10.43	9.51	10.89	10.06	11.22	11.13	11.15
F	0.04	0.10	0.01	0.05	0.06	0.00	0.12	0.01	0.02	0.05	0.12	0.04	0.07	0.06
H_2O*	4.40	4.39	4.40	4.31	4.30	4.26	4.23	4.30	4.29	4.36	4.27	4.31	4.26	4.40
Sum**	98.86	98.77	98.83	98.76	99.47	98.35	99.03	99.31	99.62	98.82	99.39	98.62	98.63	99.89
Si *apfu*	6.921	6.779	6.901	6.825	6.619	6.685	6.555	6.636	6.564	7.002	6.495	6.827	6.664	6.981
^{IV}Al	1.079	1.221	1.099	1.175	1.381	1.315	1.444	1.364	1.436	0.997	1.505	1.173	1.336	1.019
^{VI}Al	2.986	3.092	3.046	2.954	2.890	2.815	2.738	2.707	2.847	2.808	2.215	2.860	2.643	2.844
Cr	0.009	0.006	0.000	0.000	0.000	0.000	0.000	0.000	0.000	0.000	0.003	0.003	0.010	0.008
Ti	0.007	0.022	0.008	0.013	0.031	0.029	0.046	0.031	0.037	0.007	0.021	0.013	0.023	0.011
Fe^{2+}	0.368	0.380	0.352	0.427	0.514	0.534	0.441	0.462	0.498	0.368	0.129	0.515	0.404	0.368
Fe^{3+}	0.000	0.000	0.000	0.000	0.080	0.092	0.284	0.302	0.110	0.000	0.998	0.049	0.411	0.000
Mn	0.002	0.012	0.007	0.001	0.000	0.006	0.009	0.000	0.007	0.001	0.003	0.001	0.006	0.007
Mg	0.664	0.527	0.605	0.701	0.585	0.623	0.582	0.597	0.601	0.804	0.730	0.659	0.602	0.836
Ca	0.000	0.000	0.000	0.000	0.000	0.003	0.000	0.000	0.000	0.001	0.007	0.003	0.003	0.000
Ba	0.012	0.010	0.032	0.128	0.148	0.147	0.131	0.093	0.206	0.031	0.039	0.033	0.023	0.041
Na	0.054	0.087	0.071	0.063	0.084	0.107	0.096	0.089	0.104	0.025	0.051	0.059	0.073	0.050
K	1.904	1.737	1.883	1.744	1.753	1.791	1.775	1.851	1.693	1.901	1.780	1.983	1.983	1.927
F	0.015	0.044	0.004	0.024	0.025	0.000	0.052	0.004	0.007	0.022	0.053	0.017	0.031	0.026
OH	3.985	3.956	3.996	3.976	3.975	4.000	3.948	3.996	3.993	3.978	3.947	3.982	3.969	3.974
X_{Ms}	0.477	0.521	0.468	0.368	0.413	0.371	0.400	0.406	0.365	0.405	0.365	0.454	0.442	0.400
$X_{Fe-Al-Cel}$	0.166	0.165	0.172	0.181	0.180	0.192	0.148	0.159	0.174	0.150	0.041	0.189	0.141	0.156
$X_{Mg-Al-Cel}$	0.300	0.229	0.295	0.298	0.205	0.224	0.195	0.205	0.210	0.327	0.231	0.242	0.206	0.355

The proportion of cations is based on 44 valences. * The amount of H_2O is calculated. ** The sum is corrected for F; the sum of octahedrally coordinated cations is set at 4.1 to allow for an estimation of Fe^{3+}. The amount of Cl is below the detection limit. Symbols: Ms: muscovite, Fe–Al-Cel: ferro-aluminoceladonite, Mg–Al-Cel: aluminoceladonite.

TABLE A9. COMPOSITION OF SODIC–CALCIC AND CALCIC AMPHIBOLE, BAHIA MANSA, CHILE

	Sodic–calcic amphibole						Calcic amphibole						
Sample	96CH-197	96CH-197	96CH-201	96CH-205	96CH-215	96CH-217	96CH-219	96CH-191	96CH-196	96CH-197	96CH-205	96CH-215	96CH-217
Stage	I	I	I	I	I	I	I	I	I	II	II	II	II
SiO_2 wt%	50.72	47.72	51.59	49.68	52.17	51.64	54.09	53.45	53.99	50.87	53.30	51.15	52.59
TiO_2	0.08	0.14	0.08	0.11	0.01	0.06	0.05	0.20	0.04	0.06	0.04	0.04	0.00
Al_2O_3	5.09	6.41	4.69	5.94	3.99	4.51	2.76	2.96	1.49	3.50	2.60	4.12	2.98
Cr_2O_3	0.01	0.00	0.04	0.00	0.00	0.00	0.04	0.05	0.01	0.00	0.00	0.00	0.05
Fe_2O_3	11.72	7.20	11.40	8.31	7.87	8.18	6.99	3.81	1.74	6.74	7.66	6.06	4.42
FeO	8.43	13.30	8.61	11.11	8.50	10.49	7.37	11.50	12.08	9.29	8.45	10.57	9.99
MnO	1.04	0.78	1.09	0.77	0.53	0.49	0.31	0.36	0.32	0.91	1.44	0.62	0.43
MgO	10.84	9.81	10.49	10.67	12.87	11.92	15.03	13.80	14.69	13.36	13.20	12.72	13.68
CaO	6.31	9.22	5.80	7.91	7.61	7.80	8.83	11.20	11.62	10.10	8.95	9.82	9.58
Na_2O	4.07	2.76	3.97	3.43	3.17	3.53	2.54	0.79	0.70	1.76	1.98	1.96	1.82
K_2O	0.15	0.34	0.16	0.26	0.25	0.18	0.10	0.12	0.08	0.14	0.11	0.15	0.12
F	0.09	0.16	0.16	0.25	0.21	0.03	0.09	0.09	0.00	0.11	0.09	0.09	0.02
Cl	0.01	0.02	0.02	0.00	0.01	0.01	0.00	0.01	0.00	0.01	0.01	0.00	0.01
H_2O*	2.03	1.93	1.98	1.93	1.96	2.06	2.07	2.04	2.06	1.99	2.03	2.01	2.03
Sum**	100.55	99.73	100.01	100.28	99.06	100.89	100.24	100.16	98.81	98.79	99.82	99.26	97.70
Si *apfu*	7.351	7.113	7.490	7.267	7.575	7.450	7.685	7.691	7.855	7.467	7.689	7.478	7.719
^{IV}Al	0.649	0.887	0.510	0.733	0.425	0.550	0.315	0.309	0.145	0.533	0.311	0.522	0.281
Ti	0.009	0.016	0.009	0.012	0.001	0.007	0.005	0.002	0.005	0.007	0.005	0.004	0.000
^{VI}Al	0.220	0.239	0.292	0.291	0.257	0.217	0.147	0.193	0.110	0.072	0.131	0.188	0.235
Cr	0.001	0.000	0.005	0.000	0.000	0.000	0.005	0.006	0.001	0.000	0.000	0.000	0.005
Fe^{3+}	1.278	0.809	1.245	0.915	0.860	0.888	0.747	0.413	0.190	0.744	0.831	0.666	0.488
Fe^{2+}	1.022	1.657	1.046	1.359	1.032	1.265	0.876	1.384	1.469	1.141	1.019	1.292	1.227
Mn	0.127	0.099	0.133	0.095	0.065	0.060	0.037	0.044	0.039	0.113	0.176	0.077	0.053
Mg	2.341	2.179	2.270	2.326	2.785	2.563	3.183	2.959	3.185	2.923	2.838	2.772	2.993
Ca	0.980	1.472	0.902	1.240	1.184	1.206	1.344	1.726	1.811	1.588	1.383	1.538	1.507
Na	1.144	0.798	1.117	0.973	0.892	0.987	0.700	0.220	0.197	0.501	0.554	0.556	0.518
K	0.028	0.064	0.029	0.049	0.046	0.034	0.019	0.022	0.015	0.026	0.020	0.027	0.023
Cl	0.003	0.004	0.005	0.000	0.003	0.001	0.000	0.002	0.000	0.002	0.001	0.000	0.002
F	0.039	0.077	0.073	0.115	0.098	0.012	0.042	0.042	0.000	0.052	0.043	0.040	0.011
OH	1.958	1.919	1.922	1.885	1.899	1.986	1.958	1.956	2.000	1.946	1.956	1.960	1.988
X_{Tr}	0.490	0.736	0.451	0.620	0.592	0.603	0.672	0.863	0.906	0.794	0.692	0.769	0.753
X_{Gln}	0.075	0.060	0.104	0.092	0.094	0.078	0.054	0.043	0.035	0.018	0.042	0.051	0.080
X_{Rbk}	0.435	0.204	0.445	0.288	0.314	0.319	0.274	0.093	0.060	0.188	0.266	0.180	0.167

The proportion of cations is based on 46 valences and a sum of cations (except for Ca, Na, K) equal to 13, which leads to an estimation of the proportion of Fe^{3+}. * The proportion of H_2O is calculated to satisfy OH + F + Cl = 2. ** The sum is corrected for F and Cl. The symbols are taken from Kretz (1983).